

Document Version

Final published version

Licence

CC BY

Citation (APA)

Hoving, J. S., van Dalen, K. N., & Metrikine, A. V. (2026). A boundary method for the dynamic response of discrete lattices. *Engineering Analysis with Boundary Elements*, 189, Article 106835. <https://doi.org/10.1016/j.enganabound.2026.106835>

Important note

To cite this publication, please use the final published version (if applicable). Please check the document version above.

Copyright

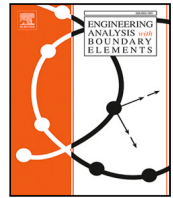
In case the licence states "Dutch Copyright Act (Article 25fa)", this publication was made available Green Open Access via the TU Delft Institutional Repository pursuant to Dutch Copyright Act (Article 25fa, the Taverne amendment). This provision does not affect copyright ownership. Unless copyright is transferred by contract or statute, it remains with the copyright holder.

Sharing and reuse

Other than for strictly personal use, it is not permitted to download, forward or distribute the text or part of it, without the consent of the author(s) and/or copyright holder(s), unless the work is under an open content license such as Creative Commons.

Takedown policy

Please contact us and provide details if you believe this document breaches copyrights. We will remove access to the work immediately and investigate your claim.



A boundary method for the dynamic response of discrete lattices[☆]

J.S. Hoving^a, K.N. van Dalen^b, A.V. Metrikine^{a,b}

^a Delft University of Technology, Faculty of Civil Engineering and Geosciences, Department Hydraulic Engineering, Section Offshore Engineering, Stevinweg 1, 2628 CN Delft, The Netherlands

^b Delft University of Technology, Faculty of Civil Engineering and Geosciences, Department Engineering Structures, Section Dynamics of Solids and Structures, Stevinweg 1, 2628 CN Delft, The Netherlands

ARTICLE INFO

Keywords:

Boundary formulations
Discrete lattices
Dynamic response
Non-smooth behaviour
Solid media

ABSTRACT

A novel boundary formulation is presented by applying the Boundary Element Method (BEM) to a dynamically loaded medium modelled as a discrete system. The two-dimensional medium is divided into a nonlinear discrete lattice in the near field, and a corresponding linear viscoelastic far field. The resulting boundary formulation is derived from the dynamic reciprocal work theorem and describes the far-field response through a Laplace domain force–displacement relation. The involved dynamic compliance matrix is composed of newly derived expressions for the Green's functions of a viscoelastic half-plane of particles.

It is demonstrated that the presented method yields a perfectly non-reflective boundary in the Laplace domain, without the need for artificial absorbing boundaries. Additionally, this contribution shows the successful time-domain application of the boundary method to a medium that exhibits non-smooth behaviour in the vicinity of a load source. In the time domain, the boundary equations are obtained by numerical application of the inverse Laplace transform, and the non-reflectiveness of the boundary is sensitive to the size of the time step. The presented method provides a consistent boundary approach for discrete lattices, and provides an alternative to continuum-based boundary methods for the dynamic response of solid media.

1. Introduction

The dynamic interaction between structures and their surroundings, such as the situation depicted in Fig. 1a, is an important aspect of many engineering problems, and a proper understanding of these interaction problems is often a necessity to take appropriate measures. Examples of such interactions are typically found in soil–structure and ice–structure interaction, e.g. [1,2]. Especially when dynamic loads inflict damage to a medium, and the response of the medium near the load source is governed by nonlinear phenomena, it is beneficial to divide the medium into two separate domains as shown in Fig. 1b; a sophisticated near-field domain that is able to account for nonlinear phenomena, and a far-field domain at such distance from the load source that its response is linear.

Non-smooth dynamic phenomena, typical for systems experiencing stick–slip or fracture require special attention. These usually occur in the load vicinity and should be captured within the near field. To model such phenomena, one may use either continuum or discrete descriptions of the considered solids. Given the fact that non-smooth phenomena are usually associated with relatively high strains, a reasonably accurate description of the solids requires to account for their

inhomogeneities, at least in the vicinity of the stick–slip or failure zone. These inhomogeneities are usually homogenized and accounted for by means of internal time and length scales. High-gradient homogenized continua [3–8] and regular lattices [9] are typical examples of such descriptions. It is difficult to say which of the two descriptions is more appropriate as both use several approximations. In this paper it is chosen to use a discrete description, which, in the subjective opinion of the authors, is somewhat more logical nowadays as it is directly governed by a system of ODEs and does not require FE discretization of a continuum that is often obtained based on a rheological (i.e. discrete) description of the basic continuum properties. In the framework of this choice, and depending on the scale of the problem under consideration, different discrete approaches may be used as categorized by Bolander et al. [10]. Options include conventional lattice models, particle-based lattice models, and the discrete element method. In this contribution, the near-field domain is modelled as a conventional two-dimensional lattice consisting of particles and rheological elements, such as springs, dashpots and dry-friction elements, used to describe the interaction between the particles.

[☆] This article is part of a Special issue entitled: 'BEM Memory of Domínguez' published in Engineering Analysis with Boundary Elements.

* Corresponding author.

E-mail addresses: j.s.hoving@tudelft.nl (J.S. Hoving), k.n.vandalen@tudelft.nl (K.N. van Dalen), a.metrikine@tudelft.nl (A.V. Metrikine).

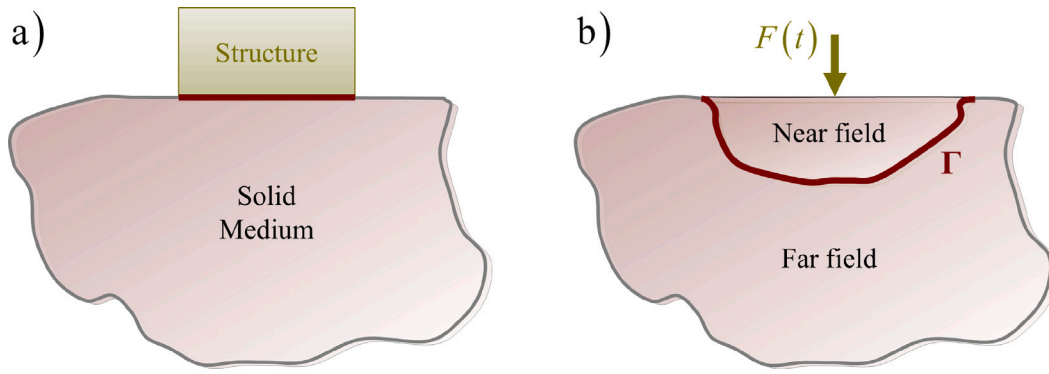


Fig. 1. (a) Interaction between a structure and its surroundings; (b) A medium divided into two domains.

To account for the response of the far-field domain, we apply the boundary element method (BEM). To achieve a boundary formulation such that there are no unwanted wave reflections at the boundary of the near-field lattice, it is most appropriate that the linear far-field domain resembles the discrete nature of the near field, and is modelled as a system of discrete particles rather than as a continuum. This is also necessary because the forces that the near-field lattice exerts on the far-field domain are point loads and it is commonly known that the response of a two-dimensional continuum under a point load is singular. Although there is some literature available regarding Green's functions for discrete lattice models, e.g. [11–13], to the knowledge of the authors, there are no publications that specifically derive boundary equations for discrete particle systems. Moreover, the development of hybrid models involving discrete lattices are very sparse in literature. The paper by Cai et al. [14] describes the coupling of two linear domains modelled by matching linear square lattices to resolve a problem in molecular dynamics. The approach described is numerically demanding and cannot be easily adapted for different geometries. Later works by Karpov et al. [15], and Carpio and Tapiador [16] present more generic approaches to determine non-reflecting boundary conditions in molecular dynamics by employing Green's functions for lattices [12]. More recently, Barbosa et al. used Green's functions for lattices to model settlement of ballast in railway track transition zones [17]. In correspondence with using PMLs [18], these approaches are aimed at developing non-reflective boundaries. The current contribution on the other hand, presents a novel boundary formulation by applying the BEM to a discrete particle system as a truthful representation of the far-field domain and its properties.

While the papers of Friedman and Shaw [19] and Banaugh and Goldsmith [20] present the first applications of the BEM in dynamics, specifically in the time and frequency domain respectively, the work by Dominguez [21] provides the first systematic and comprehensive overview on the application of BEMs to dynamic and transient problems in continua. To honour the legacy of Professor José Dominguez, this contribution extends the application of the BEM to dynamics in discrete systems.

In the following section, we present a direct boundary formulation for two-dimensional discrete particle systems starting from the dynamic reciprocal work theorem. In Section 3, the corresponding Laplace domain Green's functions are derived for a viscoelastic half-plane of particles with a hexagonal configuration. Subsequently, Section 4 demonstrates the application of the boundary method to a corresponding semi-infinite discrete particle system that exhibits non-smooth behaviour near a load source, and discusses its accuracy by simulating the non-smooth dynamic response of the resulting full medium. Finally, Section 5 summarizes the main results and conclusions of this study and addresses possible future applications of boundary formulations for lattices.

2. A direct boundary formulation for discrete particle systems

Consider the two different elastodynamic states of the far-field body V_F depicted in Fig. 2. The first state, depicted in Fig. 2a, considers the interaction of V_F with the near-field body V_N along their interface, which is denoted as Γ . The second state, depicted in Fig. 2b, is due to a set of external loads \mathbf{P} applied at the discrete particles along the cavity boundary of V_F , i.e. the interface Γ . Given that internal body forces are absent, the dynamic reciprocal work theorem, i.e. the into dynamics extended elastostatic reciprocal work theorem of Maxwell–Betti [22], yields the following relation between the displacements of, and the reaction forces at, the particles of V_F that exist along Γ for the two elastodynamic states:

$$\sum_j \tilde{\mathbf{R}}_{\Gamma,j}(s)^T \tilde{\mathbf{u}}_{p,j}(s) = \sum_j \tilde{\mathbf{R}}_{p,j}(s)^T \tilde{\mathbf{u}}_{\Gamma,j}(s) \quad (1)$$

Here, the vectors $\tilde{\mathbf{u}}_{\Gamma,j}(s)$ and $\tilde{\mathbf{R}}_{\Gamma,j}(s)$, respectively contain the displacements of particle j and the reaction forces at particle j along Γ due to the interaction with the near field. Furthermore, the vectors $\tilde{\mathbf{u}}_{p,j}(s)$ and $\tilde{\mathbf{R}}_{p,j}(s)$, respectively contain the displacements of particle j and the reaction forces at particle j along Γ due to the load vector \mathbf{P} . Here, the tilde denotes a variable in the Laplace domain and s is the complex-valued Laplace parameter.

Collecting the displacements for all particles along Γ per elastodynamic state in the displacement vectors $\tilde{\mathbf{u}}_{\Gamma}(s)$ and $\tilde{\mathbf{u}}_p(s)$, as well as collecting the corresponding reaction forces for all particles along Γ in the reaction force vectors $\tilde{\mathbf{R}}_{\Gamma}(s)$ and $\tilde{\mathbf{R}}_p(s)$, we can now generally express the dynamic reciprocal work theorem for discrete particle systems as:

$$\tilde{\mathbf{R}}_{\Gamma}(s)^T \tilde{\mathbf{u}}_p(s) = \tilde{\mathbf{R}}_p(s)^T \tilde{\mathbf{u}}_{\Gamma}(s) \quad (2)$$

Given that there are N_{Γ} particles along Γ , the displacement and reaction force vectors in Eq. (2) all have a length $2N_{\Gamma}$.

Fig. 2a shows the displacements $\tilde{\mathbf{u}}_{\Gamma}(s)$ and the reaction forces $\tilde{\mathbf{R}}_{\Gamma}(s)$ along Γ of the far-field body V_F that are due to the interaction with the near-field body V_N . Furthermore, Fig. 2b shows the displacements $\tilde{\mathbf{u}}_{p,j}(s)$ and the reaction forces $\tilde{\mathbf{R}}_{p,j}(s)$ along Γ of the far-field body V_F that are due to the external load vector \mathbf{P} . Now, according to Huygens' principle [23], the response of the far-field body V_F is indifferent to whether the near-field body V_N is present or not, as long as the response along Γ , and thereby the response of the far-field body V_F , is the same for both situations. Thus, choosing the load vector \mathbf{P} for the elastodynamic state depicted in Fig. 2b such that the displacements and reaction forces at the particles along Γ match the situation when a near-field body is present, we may consider the response due to the load vector \mathbf{P} as if it is applied inside a half-plane of particles without a cavity. The response of any particle inside the half-plane of particles due to an arbitrary load \mathbf{P} applied at an arbitrary particle in the half-plane can be described in terms of the Green's functions. Thus, the

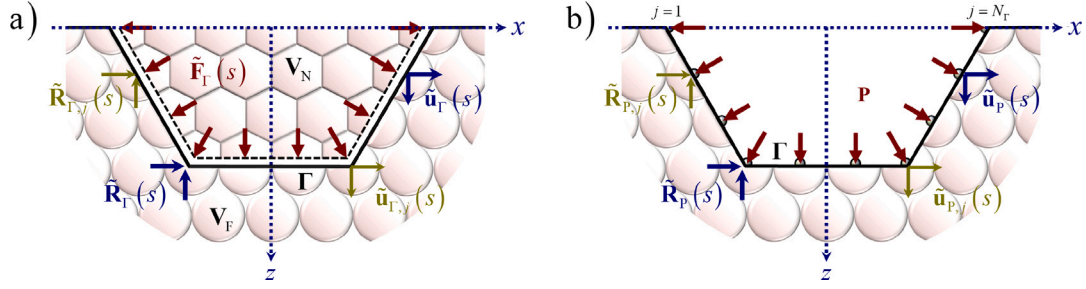


Fig. 2. Two elastodynamic states of the body V_F modelled as a discrete particle system with a hexagonal configuration: (a) Interaction with a near-field lattice; (b) Due to a set of external loads, given by the load vector \mathbf{P} .

displacements $\tilde{\mathbf{u}}_p(s)$ and the reaction forces $\tilde{\mathbf{R}}_p(s)$ for all particles along the boundary Γ due to the load vector \mathbf{P} read:

$$\tilde{\mathbf{u}}_p(s) = \tilde{\mathbf{g}}_u(s)\mathbf{P} \quad (3)$$

$$\tilde{\mathbf{R}}_p(s) = \tilde{\mathbf{g}}_R(s)\mathbf{P} \quad (4)$$

Here, $\tilde{\mathbf{g}}_u(s)$ and $\tilde{\mathbf{g}}_R(s)$ are square matrices with dimension $2N_\Gamma$ that respectively contain the Green's functions for the displacements and the reaction forces of all particles along Γ due to loads applied at all particles along Γ . For the elastodynamic state of the body V_F depicted in Fig. 2a, the reaction forces along Γ are exactly equal and opposite to the forces exerted on Γ by the near-field body V_N , in the Laplace domain denoted as $\tilde{\mathbf{F}}(s)$. The corresponding reaction forces are thus obtained as:

$$\tilde{\mathbf{R}}_\Gamma(s) = -\tilde{\mathbf{F}}(s) \quad (5)$$

Substituting Eqs. (3), (4) and (5) into the dynamic reciprocity theorem for discrete particle systems given by Eq. (2), and rearranging the remainder, yields the force–displacement relation at the particles along the boundary Γ as:

$$-\mathbf{P}^\top \tilde{\mathbf{g}}_u(s)^\top \tilde{\mathbf{F}}(s) = \mathbf{P}^\top \tilde{\mathbf{g}}_R(s)^\top \tilde{\mathbf{u}}_\Gamma(s) \quad (6)$$

Since the external load vector \mathbf{P} may be arbitrarily chosen such that all its terms are nonzero and non-infinite, we may replace it by the unit vector, which essentially removes the term \mathbf{P}^\top from Eq. (6) without violating the equality. Solving the remainder for the force vector $\tilde{\mathbf{F}}(s)$, we finally find:

$$\tilde{\mathbf{F}}(s) = -\chi(s)\tilde{\mathbf{u}}_\Gamma(s) \quad \text{with: } \chi(s) = (\tilde{\mathbf{g}}_u(s)^\top)^{-1}\tilde{\mathbf{g}}_R(s)^\top = (\tilde{\mathbf{g}}_R(s)\tilde{\mathbf{g}}_u(s)^{-1})^\top \quad (7)$$

Or inversely:

$$\tilde{\mathbf{u}}_\Gamma(s) = -\beta(s)\tilde{\mathbf{F}}(s) \quad \text{with: } \beta(s) = (\tilde{\mathbf{g}}_R(s)^\top)^{-1}\tilde{\mathbf{g}}_u(s)^\top = (\tilde{\mathbf{g}}_u(s)\tilde{\mathbf{g}}_R(s)^{-1})^\top \quad (8)$$

Here, $\chi(s)$ and $\beta(s)$ are, respectively, the dynamic stiffness matrix and the dynamic compliance matrix that both describe the Laplace domain force–displacement relation at the boundary Γ .

3. Green's functions for a viscoelastic half-plane of particles

To derive the Laplace domain Green's functions for the displacements and the reaction forces in the viscoelastic half-plane of particles,

we start from the equations of motion for a particle inside the half-plane, as depicted in Fig. 3a. The time domain equations of motion for a particle in the interior of an elastic hexagonal lattice may be derived using Lagrange's formalism [24,25] and are commonly available in literature, e.g. [26,27]. The corresponding viscoelastic equations are then obtained replacing the stiffness K_e by the operator $K_e + C_e \frac{\partial}{\partial t}$. For ease of analysis of the half-plane of particles, we normalize the equations of motion by introducing dimensionless parameters for time, as $t = t_{\text{dim}}\omega_0$, and space, as $u = u_{\text{dim}}/\ell$, where the subscript dim denotes a variable as dimensional. Furthermore, ω_0 is the particle frequency, i.e. the undamped natural frequency of a particle inside the lattice for the particular case that the motion of any adjacent particles is impeded, which for a hexagonal lattice configuration reads $\omega_0 = \sqrt{3K_e/M}$. Finally, ℓ is the interparticle distance. Inserting the given dimensionless parameters, dividing by $M\omega_0^2\ell$, and subsequently applying the Laplace transform with respect to time, the Laplace domain equations of motion for the horizontal and vertical motion of a particle m, n in the interior of the half-plane with a hexagonal configuration are found by Eqs. (9) and (10) as given in Box I.

Here, the damping ratio ζ is defined as $\zeta = C_e/C_{\text{crit}}$, where the critical particle damping C_{crit} is obtained as $C_{\text{crit}} = \frac{2}{3}M\omega_0$ for a hexagonal lattice configuration.

3.1. Governing Laplace domain displacements of the particles in the half-plane

To describe the wave propagation in the half-plane of particles due to a load \mathbf{P}^i applied at an arbitrary particle i , we seek a general solution to Eqs. (9) and (10) in the form of a superposition of plane harmonic waves [28]. To this purpose, we first introduce the Kronecker Delta $\delta_{m_i, m}$ as a means to incorporate the load \mathbf{P}^i applied at an arbitrary particle i into an interface condition along the horizontal level of particles with nodal coordinate n_i . The Kronecker Delta $\delta_{m_i, m}$ is defined as equal to one when $m = m_i$ and equal to zero when $m \neq m_i$. The load \mathbf{P}^i applied at particle i along a horizontal level of particles, may thus be expressed as $\mathbf{P}^i = \mathbf{P}\delta_{m_i, m}$. Then, noting that the given definition for the Kronecker delta has to be obeyed only at the particles, we describe the Kronecker delta by an integral identity in terms of the dimensionless horizontal wavenumber κ_x . Accounting for the horizontal spacing of the particles by describing the dimensionless x -coordinate of a particle

$$s^2 \tilde{u}_x^{m,n} + \frac{1+2\zeta s}{3} \left(3\tilde{u}_x^{m,n} - \tilde{u}_x^{m-2,n} - \tilde{u}_x^{m+2,n} - \frac{1}{4} (\tilde{u}_x^{m-1,n+1} + \tilde{u}_x^{m+1,n+1} + \tilde{u}_x^{m-1,n-1} + \tilde{u}_x^{m+1,n-1}) + \frac{\sqrt{3}}{4} (\tilde{u}_z^{m-1,n+1} - \tilde{u}_z^{m+1,n+1} - \tilde{u}_z^{m-1,n-1} + \tilde{u}_z^{m+1,n-1}) \right) = 0 \quad (9)$$

$$s^2 \tilde{u}_z^{m,n} + \frac{1+2\zeta s}{3} \left(3\tilde{u}_z^{m,n} + \frac{\sqrt{3}}{4} (\tilde{u}_x^{m-1,n+1} - \tilde{u}_x^{m+1,n+1} - \tilde{u}_x^{m-1,n-1} + \tilde{u}_x^{m+1,n-1}) - \frac{3}{4} (\tilde{u}_z^{m-1,n+1} + \tilde{u}_z^{m+1,n+1} + \tilde{u}_z^{m-1,n-1} + \tilde{u}_z^{m+1,n-1}) \right) = 0 \quad (10)$$

Box I.

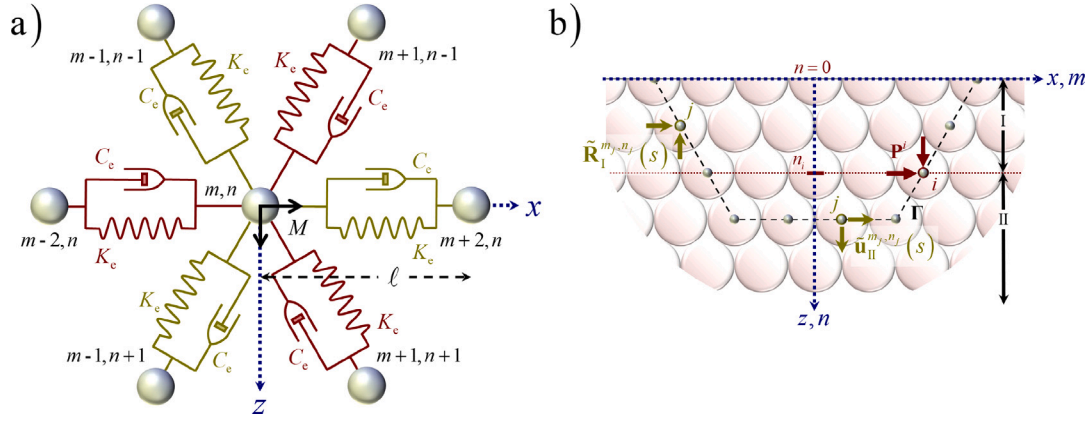


Fig. 3. (a) Hexagonal cell configuration for a particle m, n inside the viscoelastic half-plane of particles; (b) Displacements and reaction forces in the two subdomains of the half-plane of particles for a load applied at particle i .

as $x = m/2$ over an infinite horizontal domain, the Kronecker Delta may be expressed as:

$$\delta_{m_i m} = \frac{1}{4\pi} \int_{-2\pi}^{+2\pi} e^{\frac{1}{2} i \kappa_x (m_i - m)} d\kappa_x \quad (11)$$

The two-dimensional wave propagation is accounted for by additionally incorporating an exponential function related to the vertical wavenumber κ_z . Accounting for the vertical spacing of the particles by describing the dimensionless z -coordinate of a particle as $z = n\sqrt{3}/2$, as well as choosing the argument of the exponent related to κ_x in accordance with Eq. (11), the horizontal and vertical displacements of a particle m, n are described in the Laplace domain as:

$$\tilde{u}_x^{m,n} = \int_{-2\pi}^{+2\pi} A^i e^{-\frac{1}{2} i \kappa_x m} e^{+\frac{\sqrt{3}}{2} i \kappa_z n} d\kappa_x \quad (12)$$

$$\tilde{u}_z^{m,n} = \int_{-2\pi}^{+2\pi} B^i e^{-\frac{1}{2} i \kappa_x m} e^{+\frac{\sqrt{3}}{2} i \kappa_z n} d\kappa_x \quad (13)$$

Here, A^i and B^i are unknown wave amplitudes that follow from solving the system of boundary and interface conditions for the load \mathbf{P}^i as given in Section 3.3. Furthermore, note that according to the integral identity for the Kronecker Delta, the horizontal wavenumber κ_x must be real, while the vertical wavenumber κ_z may be complex-valued and depends on the horizontal wavenumber κ_x .

Eqs. (12) and (13) are expressions for the Laplace domain displacements of lattice particles, where the integral representation used is similar to the inverse Fourier integral transform with respect to the horizontal wavenumber used for continua. Thereby, the integrands in these equations can be considered as horizontal and vertical displacements in the Laplace-wavenumber domain. Substituting Eqs. (12) and (13) into Eqs. (9) and (10) for all particles yields the following system of equations for the wave amplitudes A^i and B^i :

$$\begin{aligned} \left(3 \left(1 + \frac{s^2}{1+2\zeta s} \right) - 2 \cos \kappa_x - \cos \frac{\kappa_x}{2} \cos \frac{\kappa_z \sqrt{3}}{2} \right) A^i - \sqrt{3} \sin \frac{\kappa_x}{2} \sin \frac{\kappa_z \sqrt{3}}{2} B^i &= 0 \\ -\sqrt{3} \sin \frac{\kappa_x}{2} \sin \frac{\kappa_z \sqrt{3}}{2} A^i + 3 \left(1 + \frac{s^2}{1+2\zeta s} - \cos \frac{\kappa_x}{2} \cos \frac{\kappa_z \sqrt{3}}{2} \right) B^i &= 0 \end{aligned} \quad (14)$$

The above system of homogeneous algebraic equations has a non-trivial solution if, and only if, its determinant is equal to zero. Provided that the Laplace parameter s is replaced by $i\omega$, the resulting equality, provided as Eq. (15) in Box II, gives the dispersion relation for the viscoelastic hexagonal half-plane of particles. Solving Eq. (15) for the cosine-term related to the vertical wavenumber κ_z , yields the two solutions given by Eq. (16), also provided in Box II.

In contrast to the two-dimensional isotropic continuum and the discrete particle system with a square configuration [28], it follows from

Eq. (15) that the waves propagating in a hexagonal discrete particle system are never purely shear nor purely compressional. Next, note that the two expressions provided by Eq. (16) are periodic in κ_x and that it suffices to only consider the first Brillouin zone of the lattice [29]. We denote the wavenumbers for these two expressions as $\kappa_z^{(1)}$ and $\kappa_z^{(2)}$, respectively. Using Euler's formula and the Pythagorean trigonometric identity, we find the exponents related to either wavenumber $\kappa_z^{(h)}$, with $h = 1, 2$, as:

$$e^{\pm \frac{\sqrt{3}}{2} i \kappa_z^{(h)} n} = \cos \frac{\kappa_z^{(h)} \sqrt{3}}{2} \pm i \sqrt{1 - \cos^2 \frac{\kappa_z^{(h)} \sqrt{3}}{2}} \quad (17)$$

In Eqs. (12) and (13), we have posed the Laplace domain displacements of a particle m, n in the half-plane of particles to have only one characteristic wavenumber in z -direction and we have only considered one direction of wave propagation. Clearly, there are two characteristic wavenumbers in z -direction and, depending on the location of the considered particle in the half-plane, waves may travel both in positive and in negative z -direction. Adapting Eqs. (12) and (13) to account for the two characteristic wavenumbers, as well as for the two possible direction of wave propagation, the horizontal and vertical displacements of a particle m, n due to a load at a particle i are, in a general sense, described as:

$$\tilde{u}_x^{m,n}(s) = \int_{-2\pi}^{+2\pi} \left(\sum_{h=1}^2 A_1^{i,(h)} e^{+\frac{\sqrt{3}}{2} i \kappa_z^{(h)} n} + \sum_{h=1}^2 A_2^{i,(h)} e^{-\frac{\sqrt{3}}{2} i \kappa_z^{(h)} n} \right) e^{-\frac{1}{2} i \kappa_x m} d\kappa_x \quad (18)$$

$$\tilde{u}_z^{m,n}(s) = \int_{-2\pi}^{+2\pi} \left(\sum_{h=1}^2 B_1^{i,(h)} e^{+\frac{\sqrt{3}}{2} i \kappa_z^{(h)} n} + \sum_{h=1}^2 B_2^{i,(h)} e^{-\frac{\sqrt{3}}{2} i \kappa_z^{(h)} n} \right) e^{-\frac{1}{2} i \kappa_x m} d\kappa_x \quad (19)$$

Choosing the sign of the square roots in Eqs. (16) and (17) such that the positive argument of the exponent described by Eq. (17) corresponds to waves propagating in positive z -direction, it follows that $A_1^{i,(h)}$ and $B_1^{i,(h)}$ in Eqs. (18) and (19) are the horizontal and vertical wave amplitudes of the waves propagating in positive z -direction, respectively, while $A_2^{i,(h)}$ and $B_2^{i,(h)}$ are the horizontal and vertical wave amplitudes of the waves propagating in negative z -direction, respectively.

Each wavenumber $\kappa_z^{(h)}$ corresponds to an eigenvector, where the second component of each eigenvector is obtained as $D_1^{(h)} = B_1^{i,(h)} / A_1^{i,(h)}$ for the wave propagating in positive z -direction, and as $D_2^{(h)} = B_2^{i,(h)} / A_2^{i,(h)}$ for the wave propagating in negative z -direction. Here note that, although the wave amplitudes $A_1^{i,(h)}$, $A_2^{i,(h)}$, $B_1^{i,(h)}$ and $B_2^{i,(h)}$ depend on the location of the loaded particle i , the corresponding eigenvector components do not. The resulting expressions for the two eigenvector terms follow from the system of algebraic equations for the corresponding exponents of the vertical wavenumber $\kappa_z^{(h)}$. For both vertical

$$\left(3 \left(1 + \frac{s^2}{1 + 2\zeta s}\right) - 2 \cos \kappa_x - \cos \frac{\kappa_x}{2} \cos \frac{\kappa_z \sqrt{3}}{2}\right) \left(1 + \frac{s^2}{1 + 2\zeta s} - \cos \frac{\kappa_x}{2} \cos \frac{\kappa_z \sqrt{3}}{2}\right) - \sin^2 \frac{\kappa_x}{2} \sin^2 \frac{\kappa_z \sqrt{3}}{2} = 0 \quad (15)$$

$$\left(\cos \frac{\kappa_z \sqrt{3}}{2}\right)_{1,2} = \left(2 \left(1 + \frac{s^2}{1 + 2\zeta s}\right) - \cos \kappa_x\right) \cos \frac{\kappa_x}{2} \pm \frac{1}{1 + 2\zeta s} \sqrt{s^4 (2 \cos \kappa_x - 1) - 2s^2 (1 + 2\zeta s) (\cos \kappa_x - 1)^2 + \frac{1}{2} (1 + 2\zeta s)^2 (\cos \kappa_x - 1)^3} \quad (16)$$

Box II.

wavenumbers, the resulting expressions for the two eigenvector terms are found to be related as $D_1^{(h)} = -D_2^{(h)} = D^{(h)}$, where:

$$D^{(h)} = \frac{\frac{1}{3} \sqrt{3} \sin \frac{\kappa_x}{2} \sin \frac{\kappa_z^{(h)} \sqrt{3}}{2}}{1 + \frac{s^2}{1 + 2\zeta s} - \cos \frac{\kappa_x}{2} \cos \frac{\kappa_z^{(h)} \sqrt{3}}{2}} \quad (20)$$

For the situation that a loaded particle i is located in the interior of the half-plane of particles, we must separately describe the response of the half-plane for the domain $n \in [0 \dots n_i]$, i.e. subsystem I, where waves travel in both positive and negative z -directions due to reflections from the half-plane surface, and for the domain $n \in [n_i \dots \infty]$, i.e. subsystem II, where waves only travel in positive z -direction. Fig. 3b depicts the division of the half-plane of particles into two subsystems based on the location of the loaded particle i .

Consequently, the horizontal and vertical displacements of a particle m, n in subsystem I due to a load at a particle i respectively become:

$$\tilde{u}_{x,I}^{m,n}(s) = \int_{-2\pi}^{+2\pi} \left(\sum_{h=1}^2 A_1^{i,(h)} e^{+\frac{\sqrt{3}}{2} i \kappa_z^{(h)} n} + \sum_{h=1}^2 A_2^{i,(h)} e^{-\frac{\sqrt{3}}{2} i \kappa_z^{(h)} n} \right) e^{-\frac{1}{2} i \kappa_x m} d\kappa_x \quad (21)$$

$$\tilde{u}_{z,I}^{m,n}(s) = \int_{-2\pi}^{+2\pi} \left(\sum_{h=1}^2 D^{(h)} A_1^{i,(h)} e^{+\frac{\sqrt{3}}{2} i \kappa_z^{(h)} n} - \sum_{h=1}^2 D^{(h)} A_2^{i,(h)} e^{-\frac{\sqrt{3}}{2} i \kappa_z^{(h)} n} \right) e^{-\frac{1}{2} i \kappa_x m} d\kappa_x \quad (22)$$

Accordingly, the horizontal and vertical displacements of a particle m, n in subsystem II due to a load at a particle i are respectively described as:

$$\tilde{u}_{x,II}^{m,n}(s) = \int_{-2\pi}^{+2\pi} \left(\sum_{h=1}^2 A_3^{i,(h)} e^{+\frac{\sqrt{3}}{2} i \kappa_z^{(h)} n} \right) e^{-\frac{1}{2} i \kappa_x m} d\kappa_x \quad (23)$$

$$\tilde{u}_{z,II}^{m,n}(s) = \int_{-2\pi}^{+2\pi} \left(\sum_{h=1}^2 D^{(h)} A_3^{i,(h)} e^{+\frac{\sqrt{3}}{2} i \kappa_z^{(h)} n} \right) e^{-\frac{1}{2} i \kappa_x m} d\kappa_x \quad (24)$$

For the particular case that the loaded particle i is located at the surface of the half-plane, subsystem I does not exist and the horizontal and vertical displacements of any particle m, n in the half-plane are described exclusively by Eqs. (23) and (24) respectively.

3.2. Governing Laplace domain reaction forces for the particles in the half-plane

Equivalent to tractions existing at the interface between two continuous bodies, reaction forces exist at particles located at an interface between two discrete particle systems. The reaction forces at a particle along an interface may be derived from its equations of motion, and by considering its cell configuration and thereby follow from the shape and the orientation of the interface at that particle. Here, we specifically consider reaction forces at particles along the interface Γ , so that the expressions for the reaction forces additionally depend on the location of that particle compared to the loaded particle i .

For any interface particle m, n that is located in the interior of subsystem I, i.e. for $0 \leq n < n_i$, all degrees of freedom in its cell may be considered as part of subsystem I. Thus, substituting Eqs. (21) and (22) into the equations of motion of particle m, n allows us to express the general solution for the horizontal and vertical reaction forces at

that particle as:

$$\tilde{R}_{x,I}^{m,n}(s) = \int_{-2\pi}^{+2\pi} \left(\sum_{h=1}^2 \varphi_{x;1}^{(h)} A_1^{i,(h)} e^{+\frac{\sqrt{3}}{2} i \kappa_z^{(h)} n} + \sum_{h=1}^2 \varphi_{x;2}^{(h)} A_2^{i,(h)} e^{-\frac{\sqrt{3}}{2} i \kappa_z^{(h)} n} \right) e^{-\frac{1}{2} i \kappa_x m} d\kappa_x \quad (25)$$

$$\tilde{R}_{z,I}^{m,n}(s) = \int_{-2\pi}^{+2\pi} \left(\sum_{h=1}^2 \varphi_{z;1}^{(h)} A_1^{i,(h)} e^{+\frac{\sqrt{3}}{2} i \kappa_z^{(h)} n} + \sum_{h=1}^2 \varphi_{z;2}^{(h)} A_2^{i,(h)} e^{-\frac{\sqrt{3}}{2} i \kappa_z^{(h)} n} \right) e^{-\frac{1}{2} i \kappa_x m} d\kappa_x \quad (26)$$

Here, $\varphi_{x;1}^{(h)}$, $\varphi_{x;2}^{(h)}$, $\varphi_{z;1}^{(h)}$ and $\varphi_{z;2}^{(h)}$ are expressions that depend on the cell configuration of the regarded interface particle.

Accordingly, for any interface particle m, n located in the interior of subsystem II, i.e. for $n > n_i$, all degrees of freedom in its cell may be considered as part of subsystem II. Thus, substituting Eqs. (23) and (24) into the equations of motion of particle m, n yields the general solution for the horizontal and vertical reaction forces at that particle as:

$$\tilde{R}_{x,II}^{m,n}(s) = \int_{-2\pi}^{+2\pi} \left(\sum_{h=1}^2 \varphi_{x;3}^{(h)} A_3^{i,(h)} e^{+\frac{\sqrt{3}}{2} i \kappa_z^{(h)} n} \right) e^{-\frac{1}{2} i \kappa_x m} d\kappa_x \quad (27)$$

$$\tilde{R}_{z,II}^{m,n}(s) = \int_{-2\pi}^{+2\pi} \left(\sum_{h=1}^2 \varphi_{z;3}^{(h)} A_3^{i,(h)} e^{+\frac{\sqrt{3}}{2} i \kappa_z^{(h)} n} \right) e^{-\frac{1}{2} i \kappa_x m} d\kappa_x \quad (28)$$

Here, the expression $\varphi_{x;3}^{(h)}$ and $\varphi_{z;3}^{(h)}$ again depend on the cell configuration of the regarded interface particle.

Finally, for the particular case that an interface particle m, n is located exactly at the level of the loaded particle, so that $n = n_i$, its equations of motion include degrees of freedom that belong to both subsystems. Consequently, substituting Eqs. (21) to (24) into the equations of motion of particle m, n then yields the general solution for the corresponding horizontal and vertical reaction forces as:

$$\tilde{R}_{x,I \cup II}^{m,n}(s) = \int_{-2\pi}^{+2\pi} \left(\sum_{h=1}^2 \left(\varphi_{x;1}^{(h)} A_1^{i,(h)} + \varphi_{x;3}^{(h)} A_3^{i,(h)} \right) e^{+\frac{\sqrt{3}}{2} i \kappa_z^{(h)} n} + \sum_{h=1}^2 \varphi_{x;2}^{(h)} A_2^{i,(h)} e^{-\frac{\sqrt{3}}{2} i \kappa_z^{(h)} n} \right) e^{-\frac{1}{2} i \kappa_x m} d\kappa_x \quad (29)$$

$$\tilde{R}_{z,I \cup II}^{m,n}(s) = \int_{-2\pi}^{+2\pi} \left(\sum_{h=1}^2 \left(\varphi_{z;1}^{(h)} A_1^{i,(h)} + \varphi_{z;3}^{(h)} A_3^{i,(h)} \right) e^{+\frac{\sqrt{3}}{2} i \kappa_z^{(h)} n} + \sum_{h=1}^2 \varphi_{z;2}^{(h)} A_2^{i,(h)} e^{-\frac{\sqrt{3}}{2} i \kappa_z^{(h)} n} \right) e^{-\frac{1}{2} i \kappa_x m} d\kappa_x \quad (30)$$

The expressions for $\varphi_{x;r}^{(h)}$ and $\varphi_{z;r}^{(h)}$ with $r = 1..3$ in Eqs. (25) to (30) are given in Appendix. Finally, note that the dependency on the position of a particle m, n relative to a loaded particle is incorporated in the expressions for the wave amplitudes as discussed below.

3.3. Boundary and interface conditions for the half-plane of particles

The expressions for the wave amplitudes $A_1^{i,(h)}$, $A_2^{i,(h)}$, and $A_3^{i,(h)}$ that correspond to the wavenumbers $\kappa_z^{(h)}$ for $h = 1, 2$ are obtained from the set of boundary and interface conditions for the half-plane of particles. For the case that the loaded particle i is located in the interior of the

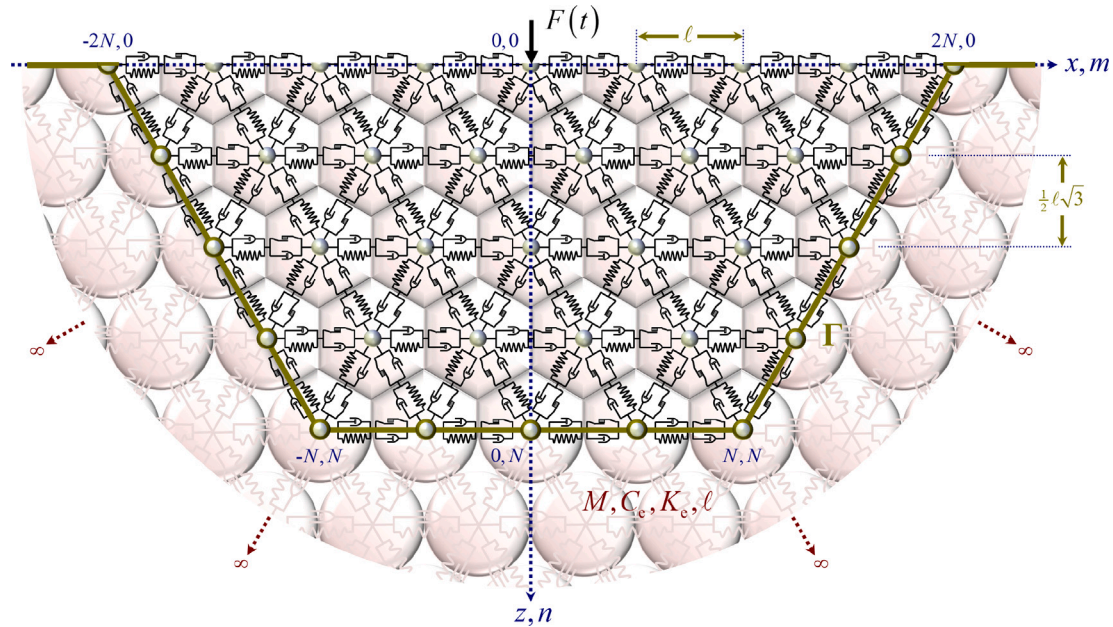


Fig. 4. A two-dimensional fully discrete system consisting of a hexagonal BKV lattice in the near field and a viscoelastic half-plane of particles in the far field.

half-plane, these conditions are:

$$\tilde{R}_{x,I}^{m,0}(s) = \tilde{R}_{x,I}^{m,0}(s) = 0 \quad (31)$$

$$\tilde{u}_{x,II}^{m,n_i}(s) - \tilde{u}_{x,I}^{m,n_i}(s) = 0 \quad (32)$$

$$\tilde{u}_{z,II}^{m,n_i}(s) - \tilde{u}_{z,I}^{m,n_i}(s) = 0 \quad (33)$$

$$\tilde{R}_{x,II}^{m,n_i}(s) - \tilde{R}_{x,I}^{m,n_i}(s) = P_x \delta_{m_i m} \quad (34)$$

$$\tilde{R}_{z,II}^{m,n_i}(s) - \tilde{R}_{z,I}^{m,n_i}(s) = P_z \delta_{m_i m} \quad (35)$$

Here, P_x and P_z are respectively the horizontal and vertical components of the point load applied at particle i , and $\delta_{m_i m}$ denotes the Kronecker Delta. The above conditions are formulated by noting that, for a load at a particle in the interior of the half-plane, there are no forces at the surface of the half-plane, the displacements of both subsystems must match at the level of the loaded particle, i.e. at $n = n_i$, and that there should be force equilibrium at the interface between the two subsystems at $n = n_i$.

For the particular case that the loaded particle i is located at the surface of the half-plane of particles, the half-plane exclusively consists of subsystem II, so that the system of boundary and interface conditions consists of only two algebraic equations that match Eqs. (34) and (35) for the case that $n_i = 0$ and by substituting $\tilde{R}_{x,I}^{m,0}(s) = \tilde{R}_{z,I}^{m,0}(s) = 0$.

3.4. Resulting Green's matrices for the displacements and reaction forces

The Green's matrices $\tilde{g}_u(s)$ and $\tilde{g}_R(s)$, appearing in the expressions for the dynamic stiffness matrix and the dynamic compliance matrix given by Eqs. (7) and (8), respectively contain the Green's functions for the displacements and the reaction forces of all particles along Γ due to loads applied at all particles along Γ . The green's functions for the displacements and the reaction forces of an arbitrary particle j along Γ with nodal coordinates m_j, n_j , due to a load applied at a particle i along Γ with nodal coordinates m_i, n_i then respectively read:

$$\tilde{g}_u^{j,i}(s) = \begin{bmatrix} \tilde{g}_{u,xx}^{j,i}(s) & \tilde{g}_{u,xz}^{j,i}(s) \\ \tilde{g}_{u,zx}^{j,i}(s) & \tilde{g}_{u,zz}^{j,i}(s) \end{bmatrix} \quad \tilde{g}_R^{j,i}(s) = \begin{bmatrix} \tilde{g}_{R,xx}^{j,i}(s) & \tilde{g}_{R,xz}^{j,i}(s) \\ \tilde{g}_{R,zx}^{j,i}(s) & \tilde{g}_{R,zz}^{j,i}(s) \end{bmatrix} \quad (36)$$

Within discrete particle systems, the Green's functions for the displacements can be straightforwardly defined as the displacements due to a unit point load. Thus, the Green's functions $\tilde{g}_{u,xx}^{j,i}(s)$ and $\tilde{g}_{u,zx}^{j,i}(s)$ are equal to the Laplace domain displacements, given by Eqs. (20) to (23),

for the case that the wave amplitudes follow from solving the system of boundary and interface conditions for $P_x = 1$ and $P_z = 0$. Accordingly, solving the system of boundary and interface conditions for $P_x = 0$ and $P_z = 1$ yields the Laplace domain displacements as the Green's functions $\tilde{g}_{u,xz}^{j,i}(s)$ and $\tilde{g}_{u,zz}^{j,i}(s)$. Using the same approach, the Green's functions for the reaction forces follow from the Laplace domain reaction forces given by Eqs. (25) to (30).

4. Application of the boundary method to a nonlinear discrete lattice

This section applies the presented boundary method to a semi-infinite discrete particle system that exhibits non-smooth behaviour close to a load source, with the aim to demonstrate that the resulting boundary formulation correctly accounts for the presence of the far-field domain, as well as discussing its accuracy. To this purpose, the near field is modelled as a lattice capable of describing non-smooth phenomena in the time domain, while the far field is described as a viscoelastic half-plane of particles. The resulting semi-infinite system is depicted in Fig. 4.

4.1. Governing equations for the nonlinear near-field lattice

To eliminate any unwanted wave reflections from the interface Γ , the geometry of the cells in the near-field lattice and in the far-field half-plane of particles match, and additionally the linear material parameters of the near-field lattice match the material parameters of the half-plane. The position of the particles in the hexagonal near-field lattice is given by nodal coordinates m, n , and every particle has mass $M^{m,n}$. To prevent dependency on the regular discretization of the lattice, and to capture the unstructured character of material behaviour, random heterogeneity is incorporated in the lattice by randomly perturbing the initial location of the particles in the lattice interior.

To allow for non-smooth behaviour, the interaction between adjacent particles in the near-field lattice is described by so-called Bingham–Kelvin–Voigt (BKV) elements that consist of a viscoelastic Kelvin–Voigt element and a Bingham element in series. The resulting configuration for a cell of a particle inside the near-field BKV lattice is depicted in

Fig. 5a. The Bingham element describes a nonlinear viscoplastic relation as a parallel combination of a dashpot and a dry-friction element. Dry-friction elements are activated only when the force working on the dry-friction element is larger than a constant threshold force, here referred to as the critical friction force. That means that when the force on the dry-friction element is smaller than its threshold, the dry-friction element is not activated, the Bingham element can be considered to be rigid and the BKV element behaves as a Kelvin–Voigt element. Each particle m, n has j adjacent particles with nodal coordinates m_j, n_j , and its cell includes j BKV elements. For each BKV element between particle m, n and an adjacent particle m_j, n_j , the Kelvin–Voigt element has a stiffness coefficient $K_{e;j}^{m,n}$ and a damping coefficient $C_{e;j}^{m,n}$, while the Bingham element has a damping coefficient $C_{f;j}^{m,n}$ and a critical friction force $F_{cr;j}^{m,n}$. As depicted in **Fig. 5a**, the BKV elements in a cell of a particle m, n have two different orientations to make sure that it represents a unit cell for the whole lattice.

Rheological elements that feature dry-friction elements behave differently depending on whether the dry-friction element is activated or not; when the dry-friction element is not activated this is referred to as ‘stick’, while the motion state for which the dry-friction element is activated is referred to as ‘slip’. Next to stick and slip, we additionally introduce a motion state to the near-field lattice, that we refer to as ‘lock’. This lock-state considers the inelastic collision of two particles; if two particles collide their relative motion is impeded and the rheological element between these particles can be considered rigid until their relative motion is reversed. This lock-state is not represented graphically in **Fig. 5a** as the behaviour of this motion state is independent of the configuration of the rheological element. Stick, slip and lock each yield different equations of motion depending on the rheological element in which these motion states occurs.

The motion states of all BKV elements at the surface and in the interior of the near-field lattice may change and vary individually, so that different BKV elements in a cell may simultaneously be in different motion states. Accounting for the two different orientations of the BKV elements in a cell, as well as accounting for the variation in motion states, the general governing equations of motion for any free particle read:

$$M^{m,n} \ddot{u}_x^{m,n} - \sum_{j \in j_{KV}^{m,n}} \left(C_{e;j}^{m,n} \dot{e}_{s;j}^{m,n} + K_{e;j}^{m,n} e_{s;j}^{m,n} \right) \cos \alpha_j^{m,n} - \sum_{j \in j_B^{m,n}} F_{s;j}^{m,n} \cos \alpha_j^{m,n} - \sum_{j \in j_{lock}^{m,n}} F_{l;j}^{m,n} \cos \alpha_j^{m,n} = 0 \quad (37)$$

$$M^{m,n} \ddot{u}_z^{m,n} - \sum_{j \in j_{KV}^{m,n}} \left(C_{e;j}^{m,n} \dot{e}_{s;j}^{m,n} + K_{e;j}^{m,n} e_{s;j}^{m,n} \right) \sin \alpha_j^{m,n} - \sum_{j \in j_B^{m,n}} F_{s;j}^{m,n} \sin \alpha_j^{m,n} - \sum_{j \in j_{lock}^{m,n}} F_{l;j}^{m,n} \cos \alpha_j^{m,n} = 0 \quad (38)$$

Here, $j_{KV}^{m,n}$ and $j_B^{m,n}$ denote the set of BKV elements in the cell that, respectively, have the Kelvin–Voigt element or the Bingham element directly connected to the particle m, n , while $j_{lock}^{m,n}$ denotes the set of elements in the cell that are in lock. Furthermore, note that the elongation $e_{s;j}^{m,n}$, the elongation rate $\dot{e}_{s;j}^{m,n}$, as well as the forces $F_{s;j}^{m,n}$ and $F_{l;j}^{m,n}$ all depend on the motion state of the considered BKV element. The corresponding expressions are provided by Eqs. (39) to (40), as given in **Box III**, for each of the motion states respectively.

For any BKV element in slip, the slip-node intermediate particles m, n and m_j, n_j is a degree of freedom and the following equation of motion must be added to the system of equations of motion:

$$C_{e;j}^{m,n} \dot{e}_{KV;j}^{m,n} + K_{e;j}^{m,n} e_{KV;j}^{m,n} - C_{f;j}^{m,n} \dot{e}_{B;j}^{m,n} - F_{cr;j}^{m,n} \operatorname{sgn} F_{B:slip;j}^{m,n} = 0 \quad (42)$$

In the above equations, e_j refers to the elongation of the whole BKV element, while the subscripts B and KV refer to the Bingham and Kelvin–Voigt elements. Furthermore, $e_{B;j}$ denotes the total elongation of the Bingham element that has occurred due to all occurrences of slip prior to the current motion state. In the third term, $K_{l;j}^{m,n}$ is the stiffness of an additional spring that is placed parallel to the BKV element to significantly reduce the relative motion between the particles m, n and m_j, n_j , $\Delta d_j^{m,n}$ is the contraction at which lock occurs, and $F_{l;j}^{m,n}$ gives the force in that spring. The stiffness of this additional spring is chosen to be only several times larger than the stiffness of the spring in the BKV element, because this is more than sufficient to significantly reduce the relative motion between the particles m, n and m_j, n_j , and choosing this stiffness too large will lead to ill-conditioned matrices in the system of differential equations.

Here note that every time a state-transition occurs, the above system of equations of motion for the hexagonal BKV lattice must be updated. The transition from stick to slip occurs when the total force that is applied to the Bingham element exceeds the threshold of the dry friction element, i.e. when $|F_{B;j}^{m,n}| > F_{cr;j}^{m,n}$. The transition from slip to stick occurs when the elongation rate of the Bingham element becomes equal to zero or changes sign, i.e. when $\operatorname{sgn} \dot{e}_{B;j}^{m,n}(t) \neq \operatorname{sgn} \dot{e}_{B;j}^{m,n}(t - dt)$. The transition into lock occurs when the distance between particles m, n and m_j, n_j becomes smaller than a minimum or threshold distance, i.e. when $d_j^{m,n} \leq d_{min;j}^{m,n}$. Finally, the transition out of lock occurs when the involved particles start moving away from each other, i.e. when $\dot{e}_j^{m,n} \geq 0$.

Finally note, that as the lattice deforms, the angles of all rheological elements in the lattice, and thereby the equations of motions, change over time. Because the displacements and elongations in the hexagonal BKV lattice can be significant these geometrical nonlinearities must be accounted for. Instead of considering these angles as degrees of freedom, which would yield a system of nonlinear equations, we assume the angles of all rheological elements as constants during each time step, and update these angles after each time step.

Accounting for the different motion states, the system of equations of motion for all free particles in the near-field lattice, i.e. all particles not located at the lattice boundary, may generally be expressed as:

$$\mathbf{M}_{fr} \ddot{\mathbf{u}}_{fr} + \mathbf{C}_{fr} \dot{\mathbf{u}} + \mathbf{K}_{fr} \mathbf{u} + \mathbf{F}_{cr:fr} = \mathbf{F}_{ext} \quad (43)$$

Here, \mathbf{M}_{fr} , \mathbf{C}_{fr} and \mathbf{K}_{fr} are respectively the mass, damping and stiffness matrices for the free particles the lattice, while $\mathbf{F}_{cr:fr}$ contains all terms related to the critical friction force in the Bingham elements and \mathbf{F}_{ext} includes any externally applied forces.

4.2. Properties of the interface and the governing boundary equations

The location of the interface Γ between the lattice and the half-plane is chosen at such a distance from the origin that nonlinearities due to a load at the origin only occur in the near-field and never occur at or beyond the interface. The domain in which these nonlinearities can

stick:	$e_{s;j}^{m,n} = e_j^{m,n} - \varepsilon_{B;j}^{m,n}$,	$F_{s;j}^{m,n} = C_{e;j}^{m,n} \dot{e}_{s;j}^{m,n} + K_{e;j}^{m,n} e_{s;j}^{m,n}$,	$F_{l;j}^{m,n} = 0$	(39)
slip:	$e_{s;j}^{m,n} = e_{KV;j}^{m,n} - \varepsilon_{B;j}^{m,n}$,	$F_{s;j}^{m,n} = C_{f;j}^{m,n} \dot{e}_{B;j}^{m,n} + F_{cr;j}^{m,n} \operatorname{sgn} F_{B:slip;j}^{m,n}$,	$F_{l;j}^{m,n} = 0$	(40)
lock:	$e_{s;j}^{m,n} = e_j^{m,n} - \varepsilon_{B;j}^{m,n}$,	$F_{s;j}^{m,n} = C_{e;j}^{m,n} \dot{e}_{s;j}^{m,n} + K_{e;j}^{m,n} e_{s;j}^{m,n}$,	$F_{l;j}^{m,n} = K_{l;j}^{m,n} \left(e_j^{m,n} + \Delta d_j^{m,n} \right)$	(41)

Box III.

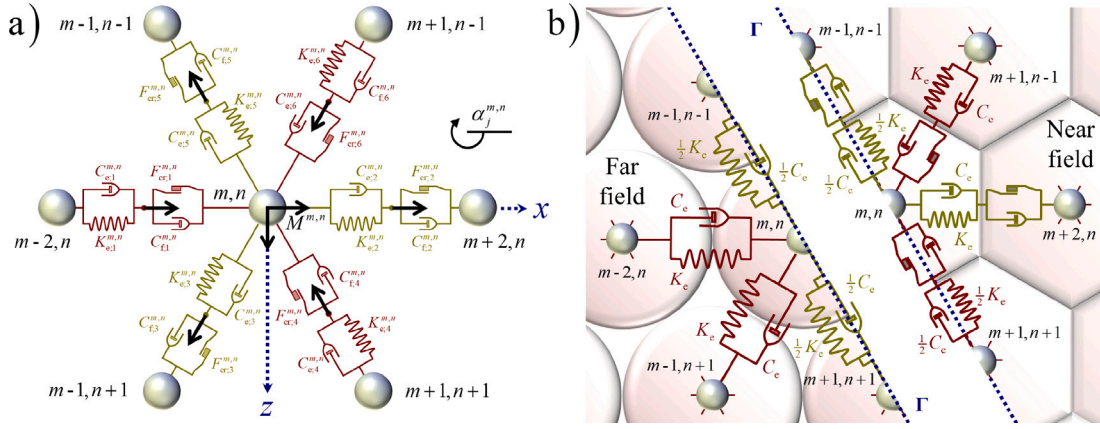


Fig. 5. Hexagonal cell configuration for a particle m,n : (a) in the interior of the nonlinear BKV lattice in the near field; (b) at the interface Γ between the near field and the far field.

occur is limited due to energy dissipation and geometrical spreading. The distance between the origin of the near-field lattice and any particle at the interface Γ is bridged by n rheological elements, where n equals the nodal coordinate of the horizontal segment of the interface. Fig. 4 shows the hexagonal shape of the interface Γ that results from connecting all boundary particles by straight lines. This shape of the interface may seem evident, but is only possible because of the discrete nature of the model and the reaction forces existing only at these boundary particles. As nonlinearities do not occur at the interface, the BKV elements connected to the interface behave as Kelvin–Voigt elements. The stiffness and damping of these BKV elements, respectively, match the stiffness and damping of the Kelvin–Voigt elements in the viscoelastic far field.

The hexagons in Fig. 4 illustrate the area that each particle in the near field represents. Clearly, the particles at the boundary and at the surface represent a different area as the particles in the interior of the lattice. Based on the area of the cells of these particles, their relative masses can straightforwardly be determined. For example, the surface particles and the particles along the straight segments of the boundary all have half the mass of an interior particle, while the surface boundary particles, with nodal coordinates $|2N|, 0$, have a relative mass of $1/6$ and the corner boundary particles, with nodal coordinates $|N|, N$, have a relative mass of $1/3$. In addition, the rheological elements that are situated in between adjacent boundary particles differ from those in the interior of the lattice. The corresponding rheological elements represent only the material behaviour between the boundary particles in the near field, and not the material behaviour between the same particles of the far-field. Consequently, any rheological elements at the interface have half the stiffness and half the damping of the rheological elements in the interior of the lattice.

To account for the response of the viscoelastic half-plane of particles at the boundary Γ , the force–displacement relation, previously given in the Laplace domain by either Eq. (7) or Eq. (8), must be included in the equations of motion for the boundary particles. These boundary equations cannot be obtained in the time domain analytically and are therefore obtained by numerically applying the inverse Laplace transform. Because the terms in the dynamic stiffness matrix $\chi(s)$ increase with frequency, and numerical application of the inverse Laplace transform requires truncation of the domain of integration, we express the system of boundary equations using the dynamic compliance matrix $\beta(s)$ instead. This yields the system of boundary equations in the Laplace domain as:

$$\tilde{\mathbf{u}}_{\Gamma} + \tilde{\beta}(s) (\mathbf{M}_{\Gamma} s^2 \tilde{\mathbf{u}}_{\Gamma} + (\mathbf{C}_{\Gamma} s + \mathbf{K}_{\Gamma}) \tilde{\mathbf{u}}) = 0 \quad (44)$$

Here, \mathbf{M}_{Γ} , \mathbf{C}_{Γ} and \mathbf{K}_{Γ} are respectively the mass, damping and stiffness matrices for the particles along the boundary. Applying the inverse

Laplace transform to Eq. (44) then yields:

$$\mathbf{u}_{\Gamma} + \int_0^t \beta(t - \tau) (\mathbf{M}_{\Gamma} \ddot{\mathbf{u}}_{\Gamma} + \mathbf{C}_{\Gamma} \dot{\mathbf{u}} + \mathbf{K}_{\Gamma} \mathbf{u}) (\tau) d\tau = 0 \quad (45)$$

Here, $\beta(t)$ is the time domain dynamic compliance matrix, obtained as the inverse Laplace transform of the dynamic compliance matrix $\beta(s)$.

To include Eq. (45) in an explicit system of ordinary differential equations that can be evaluated numerically, we must isolate the acceleration terms of the boundary particles. To obtain a non-zero acceleration term at the current time t , we differentiate Eq. (45) to time twice using Leibniz’ rule for differentiation of integrals [30,31]. This yields the governing system of boundary equations in the time domain as:

$$\ddot{\mathbf{u}}_{\Gamma} + \dot{\beta}(0) (\mathbf{M}_{\Gamma} \ddot{\mathbf{u}}_{\Gamma} + \mathbf{C}_{\Gamma} \dot{\mathbf{u}} + \mathbf{K}_{\Gamma} \mathbf{u}) + \int_0^t \ddot{\beta}(t - \tau) (\mathbf{M}_{\Gamma} \ddot{\mathbf{u}}_{\Gamma} + \mathbf{C}_{\Gamma} \dot{\mathbf{u}} + \mathbf{K}_{\Gamma} \mathbf{u}) (\tau) d\tau = 0 \quad (46)$$

Here, $\dot{\beta}(0)$ is the time-domain admittance matrix at time $t = 0$ and $\ddot{\beta}(t)$ is the time derivative of the time-domain admittance matrix, or the second time derivative of the time domain dynamic compliance matrix. Note here that $\dot{\beta}(t)$ under the convolution integral does not include a Dirac function.

Together, Eqs. (43) and (46) provide the complete governing system of equations of motion for the two-dimensional discrete system depicted in Fig. 4.

4.3. Linear response due to a single-sinus pulse load

This section presents and discusses the response of the BKV system, depicted in Fig. 4, for the case that nonlinear phenomena do not occur. Given the boundary formulation that models the far-field as a viscoelastic system of particles, the resulting system represents a homogeneous medium and its response is exclusively viscoelastic. To demonstrate the correctness and accuracy of the presented boundary method, the response of the BKV system is compared to the response of a viscoelastic half-plane of particles, computed without employing a boundary formulation, which should match exactly.

The near-field domain consists of a regular hexagonal BKV-lattice with a dimension $N = 8$ as depicted in Fig. 6. The interparticle distance is $\ell = 0.2 \text{ m}$ and the third dimension is arbitrarily chosen as 1 m . The lattice parameters are chosen such that the half-plane of particles and the BKV-system both represent a soil with a density $\rho = 2000 \text{ kg/m}^3$ and a Young’s modulus $E = 20 \text{ MPa}$. Assuming plane-strain conditions, the hexagonal lattice has a fixed Poisson’s ratio $\nu = 1/4$, e.g. [32]. Furthermore, the damping ratio is chosen as $\zeta = 0.2$.

As depicted in Fig. 6, there is a vertical single-sinus pulse load applied at the origin of the lattice, i.e. at the particle with nodal coordinates $0, 0$. The sinus has an amplitude $\hat{F} = 0.1 \text{ MN}$ and a dimensionless

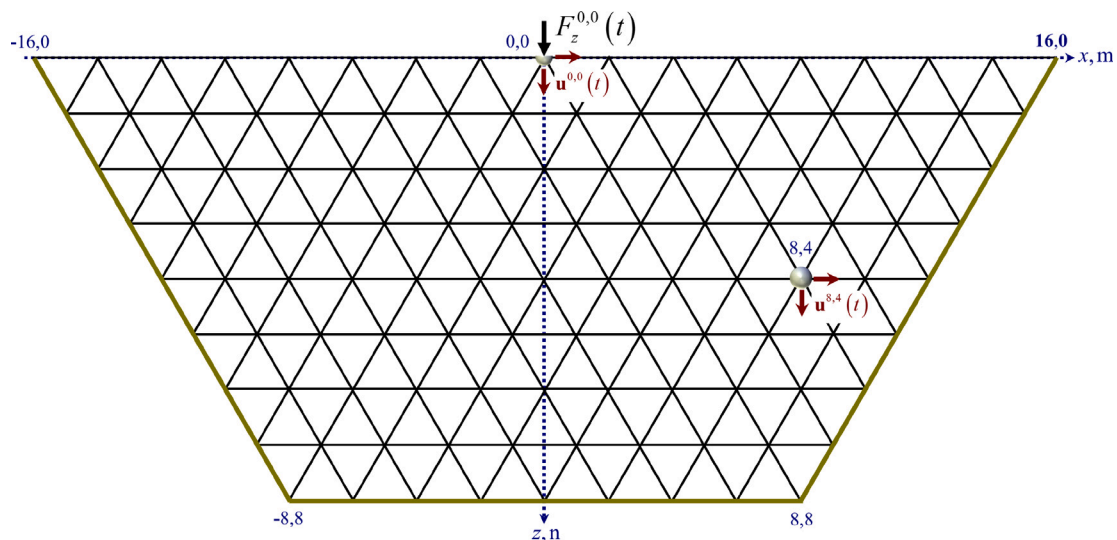


Fig. 6. A regular hexagonal lattice with dimension $N = 8$.

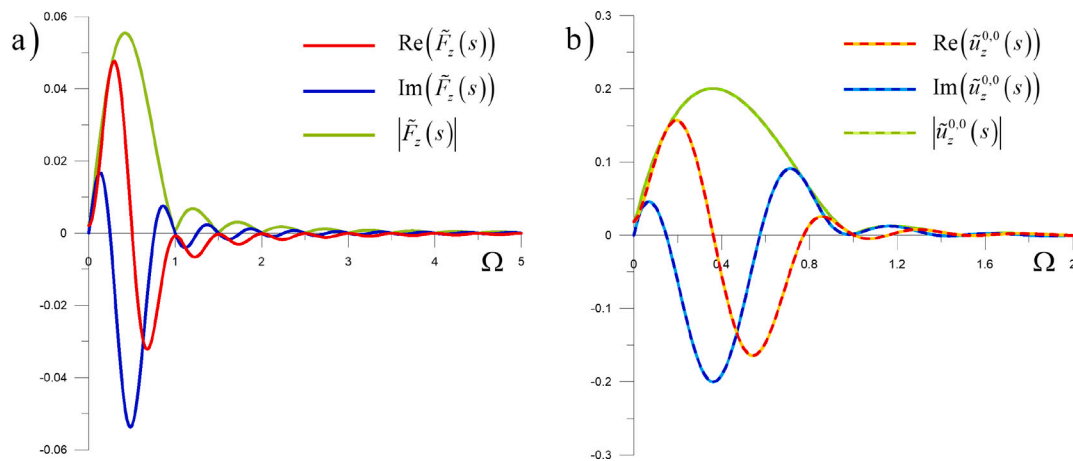


Fig. 7. (a) Laplace domain pulse load applied at particle 0,0; (b) Laplace domain displacements of particle 0,0 in the discrete half-plane (continuous) and in the linear BKV-lattice (dashed).

angular frequency $\Omega_F; = 0.5$. Fig. 7a gives the frequency dependency of the real part, the imaginary part and the absolute value of the single-sinus pulse load in the Laplace domain for the case that $s = i\Omega$, where Ω denotes the dimensionless angular frequency. The resulting vertical Laplace domain displacement response of particle 0,0 is depicted in Fig. 7b for both the BKV system and the half-plane of particles. Even though Figs. 7a and 7b are given for different frequency ranges, it is clear that the displacement response follows the loading.

Figs. 8a and 8b respectively give the horizontal and vertical Laplace domain displacements of particle 8,4 for both the BKV system and the discrete half-plane. Here, note that the location of particle 8,4 is given in Fig. 6. The continuous lines in Figs. 7b and 8 give the real part, the imaginary part and the absolute value of the Laplace domain displacements of particles 0,0 and 8,4 in the half-plane of particles, which are obtained directly from the Green's displacements of the particles in the half-plane of particles. The dashed lines in these figures give the corresponding Laplace domain displacements for the BKV system. These displacements were obtained by solving the algebraic system of Laplace domain equations of motion for the BKV system, which includes the system of boundary equations according to Eq. (44). From

the comparison of the Laplace domain displacements presented by Figs. 7b and 8, it is evident that both models yield the same displacement response in the Laplace domain. This confirms that, at least for the Laplace domain, the BKV system incorporates the behaviour of the far-field domain correctly.

Fig. 9a and Fig. 9b respectively depict the horizontal and vertical displacement response of particle 8,4 for both the half-plane of particles and the BKV system in the time domain, and for two different solution methods considered. The continuous red line gives the response for the discrete half-plane that has been obtained by taking the inverse Laplace transform of the Laplace domain displacements given in Fig. 8, while the dashed yellow line gives the response of the BKV system that has been obtained by numerically solving the system of differential equations in the time domain using the Runge–Kutta method.

Here, note that the magnitude of the displacement response of particle 8,4 is approximately ten times smaller than the displacement response of the loaded particle, i.e. particle 0,0. This decline in amplitude is attributed to both the viscous damping and the geometric damping present in the system. At the scale of these graphs, the difference between the two obtained responses is not distinguishable and the

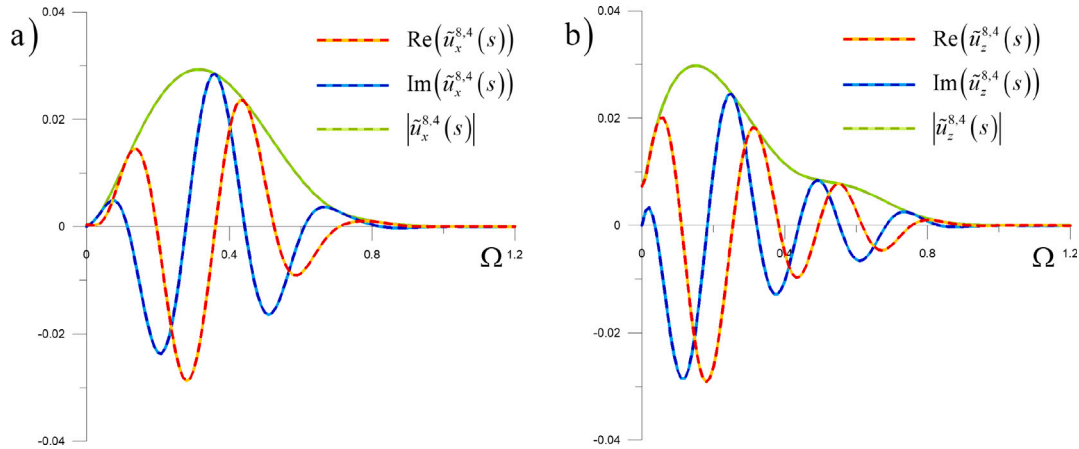


Fig. 8. Laplace domain displacements of particle 8,4 in the discrete half-plane (continuous) and the linear BKV-lattice (dashed): (a) horizontal displacements; (b) vertical displacements.

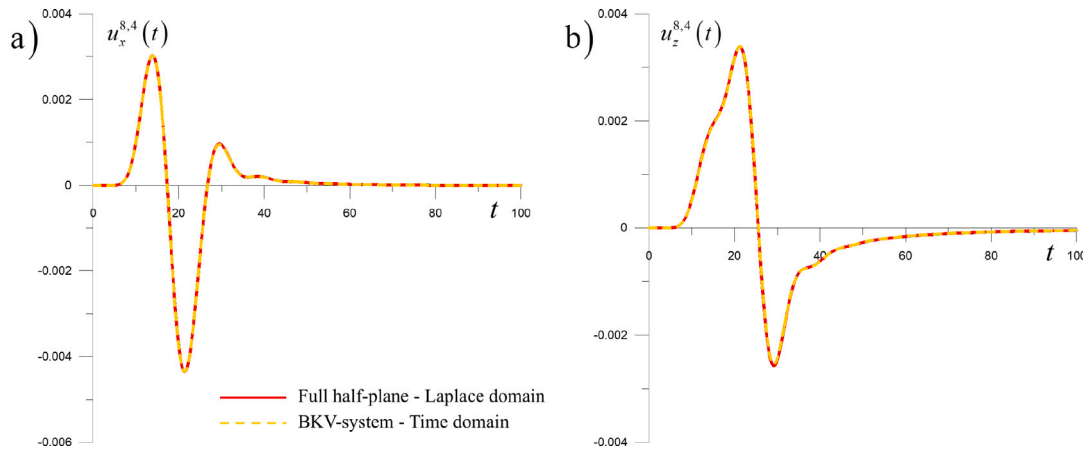


Fig. 9. Time domain displacements of particle 8,4 in the discrete half-plane (continuous) and the BKV-lattice (dashed): (a) horizontal displacements; (b) vertical displacements.

responses thus match well. Furthermore note, that the response for the BKV system shows no distinguishable reflections from the boundary.

4.4. Nonlinear response due to a single-sinus pulse load

To demonstrate that the presented boundary method also properly accounts for the behaviour of the far-field domain when nonlinearities occur in the near field, this section regards the nonlinear response of the BKV system to an externally applied time-dependent load. This section will show that, even for a nonlinear response of the near-field lattice, the proposed boundary formulation, where the far-field domain is modelled as a half-plane of particles, yields a non-reflective boundary for the BKV lattice. In Fig. 9, a comparison is given between the response obtained using a time domain approach, i.e. by solving the time domain system of ODEs, and the response obtained using a Laplace domain approach, in this case by first solving the system of equations of motion algebraically in the Laplace domain and subsequently taking the inverse Laplace transform. When nonlinearities are accounted for in the lattice, this Laplace domain approach is no longer available. In this section, we will therefore use the time domain approach to compare the response of two matching BKV systems with a near field of different dimensions, so that the boundaries of these two systems are situated at different distances from the applied load. Then, if the responses for both BKV systems match, their boundaries must be non-reflective and,

based on that, it can be concluded that the presented boundary method is correctly applied.

The matching configurations of the two BKV systems with respectively dimensions $N = 8$ and $N = 12$ are depicted in Fig. 10. The BKV lattice with dimension $N = 8$ is depicted by the black lines and its geometry is randomized using a Gauss distribution with a mean interparticle distance $\ell = 0.2$ m and a standard deviation $\ell/6$. The BKV lattice with dimension $N = 12$ is depicted by dark red lines. As the geometry of both lattices initially match, the BKV elements of the BKV lattice with dimension $N = 8$ conceals the BKV elements of the larger lattice within its own domain. Additionally, note that the geometry of the BKV lattice with dimension $N = 12$ has not been randomized beyond the domain of the BKV lattice with dimension $N = 8$, because for the smaller lattice, these particles are part of the half-plane of particles that has a regular geometry.

Both systems represent the same soil as before with a density $\rho = 2000$ kg/m³, a Young's modulus $E = 20$ MPa, a Poisson's ratio of $\nu = \frac{1}{4}$ and a damping ratio $\zeta = 0.2$. To induce stick-slip behaviour in the BKV lattice, the critical friction force of the dry friction elements in the BKV lattice is chosen relative to the amplitude of the sinus in the applied pulse load as $F_{cr} = 0.4\hat{F}$, while the threshold distance for lock is set as $d_{min} = 0.9d_0$, where d_0 is the initial distance between two adjacent particles. To enhance the probability that nonlinear phenomena occur, the BKV lattice incorporates a cluster of weak BKV elements, depicted in Fig. 10 by the red lines, that have a stiffness, a damping and a critical

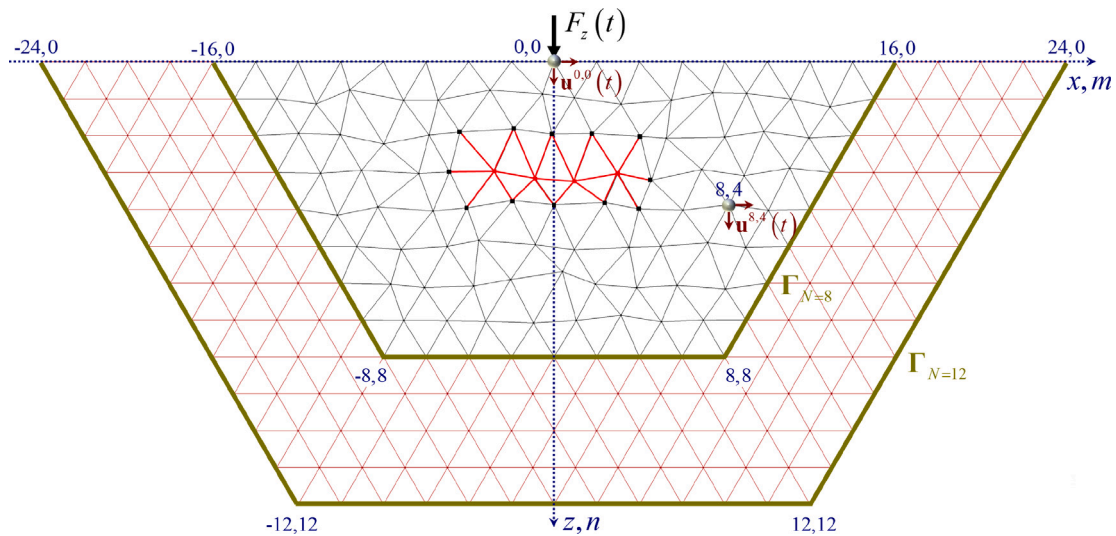


Fig. 10. Matching BKV systems with respectively dimensions $N = 8$ and $N = 12$, with the same cluster of weak BKV elements.

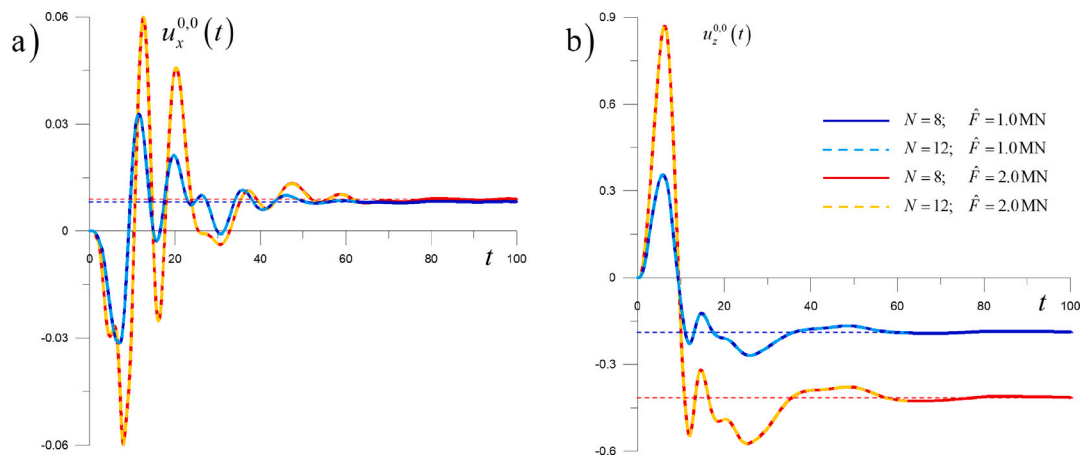


Fig. 11. Time domain response of the BKV systems with dimensions $N = 8$ and $N = 12$ for two different load amplitudes: (a) horizontal displacements of particle 0,0; (b) vertical displacements of particle 0,0.

friction force that are five times lower than the other BKV elements in the lattice.

Figs. 11 and 12 give the time domain displacement responses for the particles with nodal coordinates 0,0 and 8,4, respectively. In each figure, the displacement responses of the corresponding particles are compared for the two BKV-systems and for two different load amplitudes of a vertical single-sinus pulse load applied at the origin of the lattice. The continuous blue line gives the displacement response for the lattice with dimension $N = 8$ and a load amplitude $\hat{F} = 1.0\text{MN}$, while the dashed light-blue line gives the corresponding displacement response for the lattice with dimension $N = 12$ and the same load amplitude. Accordingly, the continuous red and the dashed dark-yellow line respectively give the displacement response for the lattices with dimension $N = 8$ and dimension $N = 12$, both for a load amplitude $\hat{F} = 2.0\text{MN}$. From evaluating the displacement responses in Figs. 11 and 12, we first and foremost observe that, at the scale of the depicted graphs, the responses of the lattices with dimension $N = 8$ and dimension $N = 12$ match exactly for both load amplitudes. Here, note that in all figures, the response of the lattice with dimension $N = 12$ is depicted only up to dimensionless time $t = 62.3$. The reason for this is that, despite using sparse matrices, the large amount of degrees of freedom in the system

with dimension $N = 12$ combined with the presence of the convolution integral in the boundary equation and the small time step required to obtain an accurate time domain response, caused the computation to run out of virtual memory and thereby caused the calculations to stop at the given time moment. From the matching responses, we can nevertheless conclude that the presented boundary method yields a non-reflective boundary and thereby correctly represents the far-field.

Next to this, the displacement responses depicted in Figs. 11 and 12 show clear evidence of nonlinear behaviour, as all responses show a permanent particle displacement after the incident waves have passed. Comparing the responses for the different particles, it is clear that the permanent deformations are most severe for the loaded particle, i.e. for particle 0,0, and in vertical direction. The deformation quickly reduces as the distance from the origin of the lattice increases. This is also clearly visible in Fig. 13 that shows the lasting deformation of the two near-field lattices at the end of the simulations. In total, 18 different BKV elements experienced one or multiple nonlinear events. In Fig. 13 these BKV elements are highlighted in blue. All these BKV elements are either close, or directly connected, to the loaded particle, or are part of the cluster of weak elements in the interior of the lattice. In total, 50 nonlinear events occurred during the simulation. Of these,

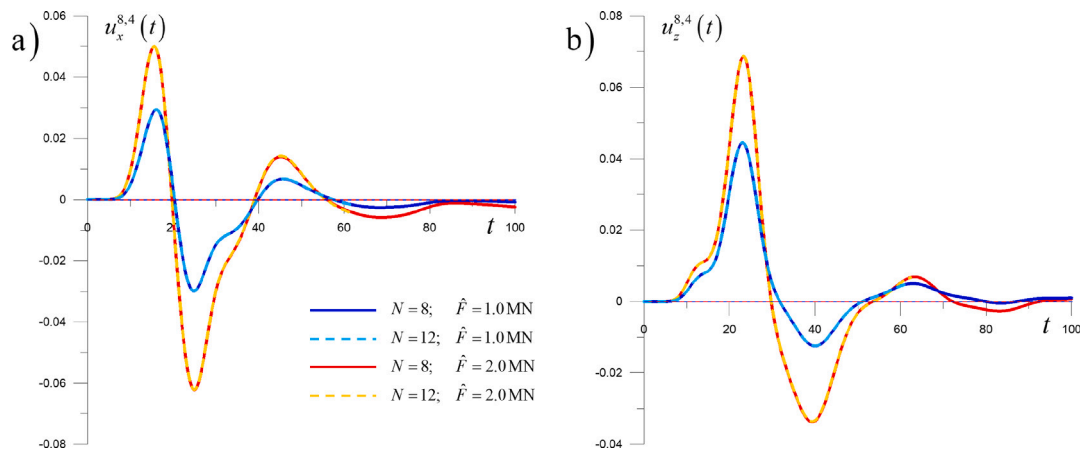


Fig. 12. Time domain response of the BKV systems with dimensions $N = 8$ and $N = 12$ for two different load amplitudes: (a) horizontal displacements of particle 8, 4; (b) vertical displacements of particle 8, 4.

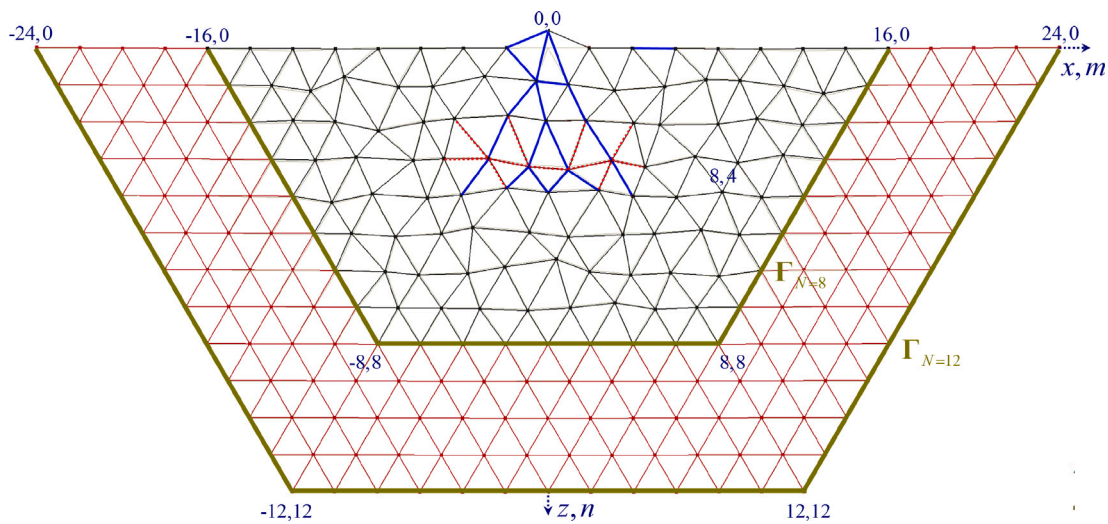


Fig. 13. Positioning of all particles and elements in the BKV lattices with dimensions $N = 8$ and $N = 12$ at the end of the simulations.

there were 19 transitions into lock, 19 lock-to-stick transitions, 6 stick-to-slip transitions and 6 slip-to-stick transitions. Since the lock-state only occurs in compression, the motion of the particles in positive z -direction is impeded, while it is not in negative z -direction. As a result of this, the permanent deformation of particle 0,0 is directed upwards in Fig. 13, and has a negative value in Fig. 11b. The fact that the permanent deformation in vertical direction of particle 0,0 is far more severe than the deformation in horizontal direction is a logical consequence of the external dynamic load having been applied vertically. Furthermore, note that the horizontal displacement response of the vertically loaded particle depicted in Fig. 11a is nonzero only because the geometry has been randomized and is only as a result of this is not symmetric in the z -axis. Furthermore, note that the loaded particle shows an oscillatory horizontal motion, which is likely due to the incident wave partially reflecting back from the edges of weak domain, where the lattice properties suddenly change, and partially reflecting back due to the occurrence of nonlinear events within the weak cluster of elements. For particle 8, 4, located outside and beyond the domain of weak elements, these oscillatory motions are hardly observed, which is likely due to the viscous and geometrical damping.

Finally, Fig. 14 shows how the total energy present in the two near-field lattices changes over time. Here, Fig. 14a compares the total energy over time in the two lattices with dimensions $N = 8$ and $N = 12$ for a single-sinus pulse load where the sinus has an amplitude

of 1.0 MN, while Fig. 14b makes the same comparison, but now for an amplitude of 2.0 MN. The continuous lines in Fig. 14 both give the total energy in the BKV lattice with dimension $N = 8$, while the dashed lines correspond to the total energy in the BKV lattice with dimension $N = 12$. For both load cases, we see that up to dimensionless time $t \approx 16$ the total energy over time is equal for both lattices. This corresponds with the moment in time at which the front of the incident wave due to the applied pulse load is observed to reach the boundary of the BKV lattice with dimension $N = 8$ and is transmitted into the corresponding far-field domain. At this time however, the front of the incident wave has not yet perceptibly reached the boundary of the BKV lattice with dimension $N = 12$ and, as a consequence, the total energy present inside is no longer the same for both lattices. The time at which the maximum of the total energy is reached in both lattices coincides with the end of the applied single-sinus pulse load. From that moment onwards, the total energy in the system declines due to viscous damping and the occurrence of nonlinear events, although most of the nonlinear events occur during the application period of the load. Many of the waves that reflect from the cluster of weak elements and from the inhomogeneity induced by nonlinear events, will first travel back to the lattice surface, before they arrive at the lattice boundary and transmit their energy into the far-field domain. As depicted in Fig. 12, it takes quite some time but eventually all the remaining energy fully

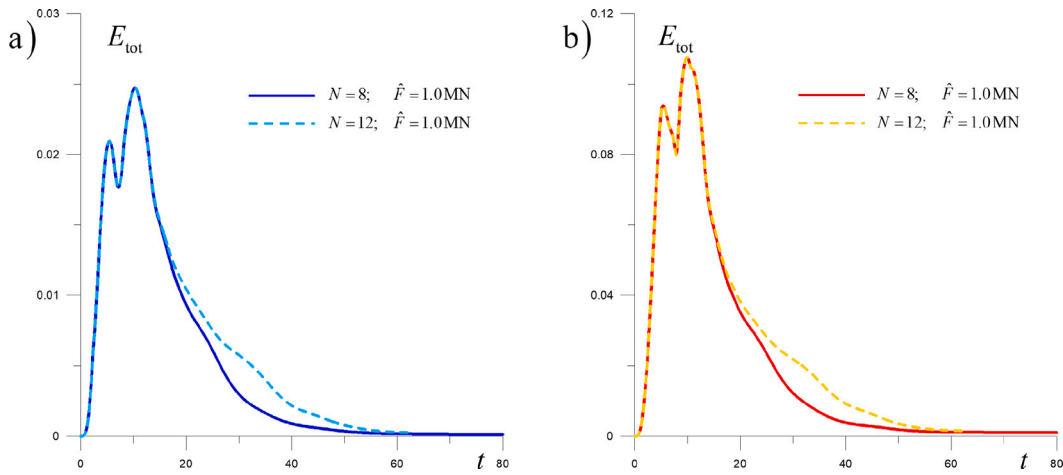


Fig. 14. Total energy present in the BKV lattices during their response, comparing the lattices with dimensions $N = 8$ and $N = 12$: (a) for a load amplitude of 1.0 MN; (b) for a load amplitude of 2.0 MN.

dissipates from the lattice, either because of viscous damping or due to the occurrence of nonlinear events.

From these findings, we conclude that the presented boundary method is not only valid for linear viscoelastic systems, but is also valid when physical and geometrical nonlinearities are accounted for. That is, as long as the boundary is sufficiently far away from the load so that both physical and geometrical nonlinearities do not occur at the boundary.

5. Conclusions

This contribution presents a boundary method for a discrete near-field domain that correctly accounts for the linear response of the far-field domain by modelling the far field as a half-plane of particles. To this purpose, the response of the far-field domain is described by a Laplace domain force–displacement relation, known as the dynamic compliance relation, at the boundary of the near field. Novel expressions for the Green’s functions for the displacements and reaction forces in the half-plane of particles, which the dynamic compliance matrix consists of, are derived and presented. Furthermore, it is demonstrated that the linear response of the near-field lattice, which is obtained by algebraically solving its Laplace domain system of equations of motion including its boundary relations, matches the response of an equivalent viscoelastic half-plane of particles exactly.

Additionally, this contribution shows the successful time-domain application of the presented boundary method to a nonlinear discrete lattice in the near-field that is able to capture non-smooth dynamic phenomena in the vicinity of a load source. By matching the material and the geometrical parameters of the discrete models that represent the near-field and far-field domains, as well as choosing the boundary of the near-field domain in the region where nonlinear phenomena no longer occur, the half-plane of particles provides a non-reflective boundary for the near-field lattice even when the near field exhibits non-smooth behaviour. To be able to numerically solve the corresponding system of ordinary differential equations in the time domain, the boundary equation must be manipulated to include a nonzero acceleration term at the current time step. Additionally, given the numerical application of the inverse Laplace transform, the accuracy of the boundary method depends on the quality of the numerical evaluation. And since the time step required to get an accurate time domain response is relatively small, time domain simulations are computationally heavy. Nevertheless, the presented method provides a consistent boundary approach for discrete lattices, and provides an alternative to continuum-based boundary methods for the dynamic response of solid media.

As an alternative to a half-plane, the discrete far-field domain may also be modelled to have a finite domain, for example by introducing a fixed bottom, resulting in reflected waves entering the near-field domain. Thereby, the methodology presented is more widely applicable than approaches solely aimed at suppressing wave reflections and introducing silent boundaries.

CRedit authorship contribution statement

J.S. Hoving: Writing – original draft & revisions, Modelling, Visualization, Investigation, Formal analysis, Data curation, Conceptualization. **K.N. van Dalen:** Writing – review & editing, Supervision, Methodology. **A.V. Metrikine:** Supervision, Resources, Methodology, Conceptualization.

Declaration of competing interest

The authors declare that they have no known competing financial interests or personal relationships that could have appeared to influence the work reported in this paper.

Appendix. Additional expressions for the reaction forces

The reaction forces given in Eqs. (25) to (30), in Section 3.2, include expressions for $\varphi_{x;r}^{(h)}$ and $\varphi_{z;r}^{(h)}$ with $r = 1..3$ that depend on the cell configuration of the particle at which the reaction forces are considered, and on the location of that particle compared to the loaded particle. Fig. 15 shows the seven cell configurations that exist along Γ .

In the following, the expressions for $\varphi_{x;r}^{(h)}$ and $\varphi_{z;r}^{(h)}$ with $r = 1..3$ are listed for all seven cell configurations. To reduce the length of the given expressions, we introduce the following notations:

$$\delta^p = 1 + D^{(h)}\sqrt{3} \quad f_x^p = \frac{1}{2} \left(\cos \frac{K_x}{2} + D^{(h)}i\sqrt{3} \sin \frac{K_x}{2} \right)$$

$$f_z^p = \frac{3}{2} \left(D^{(h)} \cos \frac{K_x}{2} + \frac{i}{\sqrt{3}} \sin \frac{K_x}{2} \right) \tag{47}$$

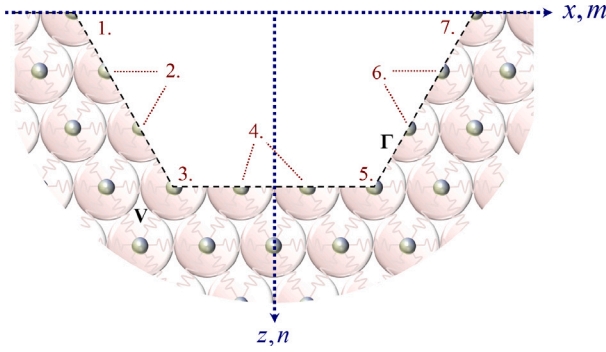
$$\delta^n = 1 - D^{(h)}\sqrt{3} \quad f_x^n = \frac{1}{2} \left(\cos \frac{K_x}{2} - D^{(h)}i\sqrt{3} \sin \frac{K_x}{2} \right)$$

$$f_z^n = \frac{3}{2} \left(D^{(h)} \cos \frac{K_x}{2} - \frac{i}{\sqrt{3}} \sin \frac{K_x}{2} \right) \tag{48}$$

For the left surface particle, these expressions are found as:

$$\varphi_{x;1/3}^{(h)} = \frac{1}{3}s^2 + \frac{1}{6}K_\zeta \left(\frac{3}{2} - e^{+ik_x} + \frac{1}{4}\delta^n - \left(\frac{1}{4}\delta^n e^{+\frac{1}{2}ik_x} + f_x^n \right) e^{+\frac{\sqrt{3}}{2}ik_z^{(h)}} \right) \tag{49}$$

$$\varphi_{x;2}^{(h)} = \frac{1}{3}s^2 + \frac{1}{6}K_\zeta \left(\frac{3}{2} - e^{+ik_x} + \frac{1}{4}\delta^p - \left(\frac{1}{4}\delta^p e^{+\frac{1}{2}ik_x} + f_x^p \right) e^{-\frac{\sqrt{3}}{2}ik_z^{(h)}} \right) \tag{50}$$



#	Cell configuration
1.	Left surface particle
2.	Particle along the left slope
3.	Left corner particle
4.	Particle along the horizontal
5.	Right corner particle
6.	Particle along the right slope
7.	Right surface particle

Fig. 15. The seven different cell configurations for the particles along the boundary.

$$\varphi_{z;1/3}^{(h)} = \frac{1}{3}s^2 D^{(h)} + \frac{1}{6}K_\zeta \left(\frac{3}{2}D^{(h)} - \frac{\sqrt{3}}{4}\delta^n + \left(\frac{\sqrt{3}}{4}\delta^n e^{+\frac{1}{2}ik_x} - f_z^n \right) e^{+\frac{\sqrt{3}}{2}ik_z^{(h)}} \right) \quad (51)$$

$$\varphi_{z;2}^{(h)} = -\frac{1}{3}s^2 D^{(h)} - \frac{1}{6}K_\zeta \left(\frac{3}{2}D^{(h)} + \frac{\sqrt{3}}{4}\delta^p - \left(\frac{\sqrt{3}}{4}\delta^p e^{+\frac{1}{2}ik_x} + f_z^p \right) e^{-\frac{\sqrt{3}}{2}ik_z^{(h)}} \right) \quad (52)$$

For particles along the left slope, and $n_i \neq n_j$, these expressions read:

$$\varphi_{x;1/3}^{(h)} = \frac{1}{2}s^2 + \frac{1}{6}K_\zeta \left(3 - 2e^{+ik_x} - \frac{1}{4}\delta^p e^{+\frac{1}{2}ik_x} e^{-\frac{\sqrt{3}}{2}ik_z^{(h)}} - \left(\frac{1}{4}\delta^n e^{+\frac{1}{2}ik_x} + f_x^n \right) e^{+\frac{\sqrt{3}}{2}ik_z^{(h)}} \right) \quad (53)$$

$$\varphi_{x;2}^{(h)} = \frac{1}{2}s^2 + \frac{1}{6}K_\zeta \left(3 - 2e^{+ik_x} - \frac{1}{4}\delta^n e^{+\frac{1}{2}ik_x} e^{+\frac{\sqrt{3}}{2}ik_z^{(h)}} - \left(\frac{1}{4}\delta^p e^{+\frac{1}{2}ik_x} + f_x^p \right) e^{-\frac{\sqrt{3}}{2}ik_z^{(h)}} \right) \quad (54)$$

$$\varphi_{z;1/3}^{(h)} = \frac{1}{2}s^2 D^{(h)} + \frac{1}{6}K_\zeta \left(3D^{(h)} - \frac{\sqrt{3}}{4}\delta^p e^{+\frac{1}{2}ik_x} e^{-\frac{\sqrt{3}}{2}ik_z^{(h)}} + \left(\frac{\sqrt{3}}{4}\delta^n e^{+\frac{1}{2}ik_x} - f_z^n \right) e^{+\frac{\sqrt{3}}{2}ik_z^{(h)}} \right) \quad (55)$$

$$\varphi_{z;2}^{(h)} = \frac{1}{2}s^2 D^{(h)} + \frac{1}{6}K_\zeta \left(3D^{(h)} + \frac{\sqrt{3}}{4}\delta^n e^{-\frac{1}{2}ik_x} e^{-\frac{\sqrt{3}}{2}ik_z^{(h)}} - \left(\frac{\sqrt{3}}{4}\delta^p e^{-\frac{1}{2}ik_x} + f_z^p \right) e^{+\frac{\sqrt{3}}{2}ik_z^{(h)}} \right) \quad (56)$$

For particles along the left slope, and $n_i = n_j$, these expressions read:

$$\varphi_{x;1}^{(h)} = \frac{1}{6}s^2 + \frac{1}{6}K_\zeta \left(1 - e^{+ik_x} + \frac{1}{4}\delta^p \left(1 - e^{+\frac{1}{2}ik_x} e^{-\frac{\sqrt{3}}{2}ik_z^{(h)}} \right) \right) \quad (57)$$

$$\varphi_{x;2}^{(h)} = \frac{1}{6}s^2 + \frac{1}{6}K_\zeta \left(1 - e^{+ik_x} + \frac{1}{4}\delta^n \left(1 - e^{+\frac{1}{2}ik_x} e^{+\frac{\sqrt{3}}{2}ik_z^{(h)}} \right) \right) \quad (58)$$

$$\varphi_{x;3}^{(h)} = \frac{1}{3}s^2 + \frac{1}{6}K_\zeta \left(\frac{3}{2} - e^{+ik_x} + \frac{1}{4}\delta^n - \left(\frac{1}{4}\delta^n e^{+\frac{1}{2}ik_x} + f_x^n \right) e^{+\frac{\sqrt{3}}{2}ik_z^{(h)}} \right) \quad (59)$$

$$\varphi_{z;1}^{(h)} = \frac{1}{6}s^2 D^{(h)} + \frac{1}{6}K_\zeta \frac{\sqrt{3}}{4}\delta^p \left(1 - e^{+\frac{1}{2}ik_x} e^{-\frac{\sqrt{3}}{2}ik_z^{(h)}} \right) \quad (60)$$

$$\varphi_{z;2}^{(h)} = -\frac{1}{6}s^2 D^{(h)} + \frac{1}{6}K_\zeta \frac{\sqrt{3}}{4}\delta^n \left(1 - e^{+\frac{1}{2}ik_x} e^{+\frac{\sqrt{3}}{2}ik_z^{(h)}} \right) \quad (61)$$

$$\varphi_{z;3}^{(h)} = \frac{1}{3}s^2 D^{(h)} + \frac{1}{6}K_\zeta \left(\frac{3}{2}D^{(h)} - \frac{\sqrt{3}}{4}\delta^n + \left(\frac{\sqrt{3}}{4}\delta^n e^{+\frac{1}{2}ik_x} - f_z^n \right) e^{+\frac{\sqrt{3}}{2}ik_z^{(h)}} \right) \quad (62)$$

For particles at the left corner particle, and $n_i \neq n_j$, these expressions read:

$$\varphi_{x;1}^{(h)} = \varphi_{x;2}^{(h)} = \varphi_{z;1}^{(h)} = \varphi_{z;2}^{(h)} = 0 \quad (63)$$

$$\varphi_{x;3}^{(h)} = \frac{2}{3}s^2 + \frac{1}{6}K_\zeta \left(4 - 2\cos \kappa_x - e^{+ik_x} + \frac{1}{4}\delta^p \left(1 - e^{+\frac{1}{2}ik_x} e^{-\frac{\sqrt{3}}{2}ik_z^{(h)}} \right) - 2f_x^n e^{+\frac{\sqrt{3}}{2}ik_z^{(h)}} \right) \quad (64)$$

$$\varphi_{z;3}^{(h)} = \frac{2}{3}s^2 D^{(h)} + \frac{1}{6}K_\zeta \left(3D^{(h)} + \frac{\sqrt{3}}{4}\delta^p \left(1 - e^{+\frac{1}{2}ik_x} e^{-\frac{\sqrt{3}}{2}ik_z^{(h)}} \right) - 2f_z^n e^{+\frac{\sqrt{3}}{2}ik_z^{(h)}} \right) \quad (65)$$

For particles at the left corner particle, and $n_i = n_j$, these expressions read:

$$\varphi_{x;1}^{(h)} = \frac{1}{6}s^2 + \frac{1}{6}K_\zeta \left(1 - e^{+ik_x} + \frac{1}{4}\delta^p \left(1 - e^{+\frac{1}{2}ik_x} e^{-\frac{\sqrt{3}}{2}ik_z^{(h)}} \right) \right) \quad (66)$$

$$\varphi_{x;2}^{(h)} = \frac{1}{6}s^2 + \frac{1}{6}K_\zeta \left(1 - e^{+ik_x} + \frac{1}{4}\delta^n \left(1 - e^{+\frac{1}{2}ik_x} e^{+\frac{\sqrt{3}}{2}ik_z^{(h)}} \right) \right) \quad (67)$$

$$\varphi_{x;3}^{(h)} = \frac{1}{2}s^2 + \frac{1}{3}K_\zeta \left(\frac{3}{2} - \cos \kappa_x - f_x^n e^{+\frac{\sqrt{3}}{2}ik_z^{(h)}} \right) \quad (68)$$

$$\varphi_{z;1}^{(h)} = \frac{1}{6}s^2 D^{(h)} + \frac{1}{6}K_\zeta \frac{\sqrt{3}}{4}\delta^p \left(1 - e^{+\frac{1}{2}ik_x} e^{-\frac{\sqrt{3}}{2}ik_z^{(h)}} \right) \quad (69)$$

$$\varphi_{z;2}^{(h)} = -\frac{1}{6}s^2 D^{(h)} + \frac{1}{6}K_\zeta \frac{\sqrt{3}}{4}\delta^n \left(1 - e^{+\frac{1}{2}ik_x} e^{+\frac{\sqrt{3}}{2}ik_z^{(h)}} \right) \quad (70)$$

$$\varphi_{z;3}^{(h)} = \frac{1}{2}s^2 D^{(h)} + \frac{1}{3}K_\zeta \left(\frac{3}{2}D^{(h)} - f_z^n e^{+\frac{\sqrt{3}}{2}ik_z^{(h)}} \right) \quad (71)$$

For particles along the horizontal domain, these expressions read:

$$\varphi_{x;1}^{(h)} = \varphi_{x;2}^{(h)} = \varphi_{z;1}^{(h)} = \varphi_{z;2}^{(h)} = 0 \quad (72)$$

$$\varphi_{x;3}^{(h)} = \frac{1}{2}s^2 + \frac{1}{3}K_\zeta \left(\frac{3}{2} - \cos \kappa_x - f_x^n e^{+\frac{\sqrt{3}}{2}ik_z^{(h)}} \right) \quad (73)$$

$$\varphi_{z;3}^{(h)} = \frac{1}{2}s^2 D^{(h)} + \frac{1}{3}K_\zeta \left(\frac{3}{2}D^{(h)} - f_z^n e^{+\frac{\sqrt{3}}{2}ik_z^{(h)}} \right) \quad (74)$$

For particles at the right corner particle, and $n_i \neq n_j$, these expressions read:

$$\varphi_{x;1}^{(h)} = \varphi_{x;2}^{(h)} = \varphi_{z;1}^{(h)} = \varphi_{z;2}^{(h)} = 0 \quad (75)$$

$$\varphi_{x;3}^{(h)} = \frac{2}{3}s^2 + \frac{1}{6}K_\zeta \left(4 - 2\cos \kappa_x - e^{-ik_x} + \frac{1}{4}\delta^n \left(1 - e^{-\frac{1}{2}ik_x} e^{-\frac{\sqrt{3}}{2}ik_z^{(h)}} \right) - 2f_x^n e^{+\frac{\sqrt{3}}{2}ik_z^{(h)}} \right) \quad (76)$$

$$\varphi_{z;3}^{(h)} = \frac{2}{3}s^2 D^{(h)} + \frac{1}{6}K_\zeta \left(3D^{(h)} - \frac{\sqrt{3}}{4}\delta^n \left(1 - e^{-\frac{1}{2}ik_x} e^{-\frac{\sqrt{3}}{2}ik_z^{(h)}} \right) - 2f_z^n e^{+\frac{\sqrt{3}}{2}ik_z^{(h)}} \right) \quad (77)$$

For particles at the right corner particle, and $n_i = n_j$, these expressions read:

$$\varphi_{x;1}^{(h)} = \frac{1}{6}s^2 + \frac{1}{6}K_\zeta \left(1 - e^{-ik_x} + \frac{1}{4}\delta^n \left(1 - e^{-\frac{1}{2}ik_x} e^{-\frac{\sqrt{3}}{2}ik_z^{(h)}} \right) \right) \quad (78)$$

$$\varphi_{x;2}^{(h)} = \frac{1}{6}s^2 + \frac{1}{6}K_\zeta \left(1 - e^{-ik_x} + \frac{1}{4}\delta^p \left(1 - e^{-\frac{1}{2}ik_x} e^{+\frac{\sqrt{3}}{2}ik_z^{(h)}} \right) \right) \quad (79)$$

$$\varphi_{x;3}^{(h)} = \frac{1}{2}s^2 + \frac{1}{3}K_\zeta \left(\frac{3}{2} - \cos \kappa_x - f_x^n e^{+\frac{\sqrt{3}}{2}ik_z^{(h)}} \right) \quad (80)$$

$$\varphi_{z;1}^{(h)} = \frac{1}{6}s^2 D^{(h)} - \frac{1}{6}K_\zeta \frac{\sqrt{3}}{4}\delta^n \left(1 - e^{-\frac{1}{2}ik_x} e^{-\frac{\sqrt{3}}{2}ik_z^{(h)}} \right) \quad (81)$$

$$\varphi_{z;2}^{(h)} = -\frac{1}{6}s^2 D^{(h)} - \frac{1}{6}K_\zeta \frac{\sqrt{3}}{4} \delta^p \left(1 - e^{-\frac{1}{2}ik_x} e^{+\frac{\sqrt{3}}{2}ik_z^{(h)}} \right) \tag{82}$$

$$\varphi_{z;3}^{(h)} = \frac{1}{2}s^2 D^{(h)} + \frac{1}{3}K_\zeta \left(\frac{3}{2}D^{(h)} - f_z^n e^{+\frac{\sqrt{3}}{2}ik_z^{(h)}} \right) \tag{83}$$

For particles along the right slope, and $n_i \neq n_j$, these expressions read:

$$\varphi_{x;1}^{(h)} = \frac{1}{2}s^2 + \frac{1}{6}K_\zeta \left(3 - 2e^{-ik_x} - \frac{1}{4}\delta^n e^{-\frac{1}{2}ik_x} e^{-\frac{\sqrt{3}}{2}ik_z^{(h)}} - \left(\frac{1}{4}\delta^p e^{-\frac{1}{2}ik_x} + f_x^n \right) e^{+\frac{\sqrt{3}}{2}ik_z^{(h)}} \right) \tag{84}$$

$$\varphi_{x;2}^{(h)} = \frac{1}{2}s^2 + \frac{1}{6}K_\zeta \left(3 - 2e^{-ik_x} - \frac{1}{4}\delta^p e^{-\frac{1}{2}ik_x} e^{+\frac{\sqrt{3}}{2}ik_z^{(h)}} - \left(\frac{1}{4}\delta^n e^{-\frac{1}{2}ik_x} + f_x^n \right) e^{-\frac{\sqrt{3}}{2}ik_z^{(h)}} \right) \tag{85}$$

$$\varphi_{x;3}^{(h)} = \frac{1}{2}s^2 + \frac{1}{6}K_\zeta \left(3 - 2e^{-ik_x} - \frac{1}{4}\delta^n e^{-\frac{1}{2}ik_x} e^{-\frac{\sqrt{3}}{2}ik_z^{(h)}} - \left(\frac{1}{4}\delta^p e^{-\frac{1}{2}ik_x} + f_x^n \right) e^{+\frac{\sqrt{3}}{2}ik_z^{(h)}} \right) \tag{86}$$

$$\varphi_{z;1}^{(h)} = \frac{1}{2}s^2 D^{(h)} + \frac{1}{6}K_\zeta \left(3D^{(h)} + \frac{\sqrt{3}}{4}\delta^p e^{-\frac{1}{2}ik_x} e^{-\frac{\sqrt{3}}{2}ik_z^{(h)}} - \left(\frac{\sqrt{3}}{4}\delta^n e^{-\frac{1}{2}ik_x} + f_z^n \right) e^{+\frac{\sqrt{3}}{2}ik_z^{(h)}} \right) \tag{87}$$

$$\varphi_{z;2}^{(h)} = -\frac{1}{2}s^2 D^{(h)} - \frac{1}{6}K_\zeta \left(3D^{(h)} - \frac{\sqrt{3}}{4}\delta^p e^{-\frac{1}{2}ik_x} e^{+\frac{\sqrt{3}}{2}ik_z^{(h)}} + \left(\frac{\sqrt{3}}{4}\delta^n e^{-\frac{1}{2}ik_x} - f_z^n \right) e^{-\frac{\sqrt{3}}{2}ik_z^{(h)}} \right) \tag{88}$$

$$\varphi_{z;3}^{(h)} = \frac{1}{2}s^2 D^{(h)} + \frac{1}{6}K_\zeta \left(3D^{(h)} + \frac{\sqrt{3}}{4}\delta^n e^{-\frac{1}{2}ik_x} e^{-\frac{\sqrt{3}}{2}ik_z^{(h)}} - \left(\frac{\sqrt{3}}{4}\delta^p e^{-\frac{1}{2}ik_x} + f_z^n \right) e^{+\frac{\sqrt{3}}{2}ik_z^{(h)}} \right) \tag{89}$$

For particles along the right slope, and $n_i = n_j$, these expressions read:

$$\varphi_{x;1}^{(h)} = \frac{1}{6}s^2 + \frac{1}{6}K_\zeta \left(1 - e^{-ik_x} + \frac{1}{4}\delta^n \left(1 - e^{-\frac{1}{2}ik_x} e^{-\frac{\sqrt{3}}{2}ik_z^{(h)}} \right) \right) \tag{90}$$

$$\varphi_{x;2}^{(h)} = \frac{1}{6}s^2 + \frac{1}{6}K_\zeta \left(1 - e^{-ik_x} + \frac{1}{4}\delta^p \left(1 - e^{-\frac{1}{2}ik_x} e^{+\frac{\sqrt{3}}{2}ik_z^{(h)}} \right) \right) \tag{91}$$

$$\varphi_{x;3}^{(h)} = \frac{1}{3}s^2 + \frac{1}{6}K_\zeta \left(\frac{3}{2} - e^{-ik_x} + \frac{1}{4}\delta^p - \left(\frac{1}{4}\delta^n e^{-\frac{1}{2}ik_x} + f_x^n \right) e^{+\frac{\sqrt{3}}{2}ik_z^{(h)}} \right) \tag{92}$$

$$\varphi_{z;1}^{(h)} = \frac{1}{6}s^2 D^{(h)} - \frac{1}{6}K_\zeta \frac{\sqrt{3}}{4} \delta^n \left(1 - e^{-\frac{1}{2}ik_x} e^{-\frac{\sqrt{3}}{2}ik_z^{(h)}} \right) \tag{93}$$

$$\varphi_{z;2}^{(h)} = -\frac{1}{6}s^2 D^{(h)} - \frac{1}{6}K_\zeta \frac{\sqrt{3}}{4} \delta^p \left(1 - e^{-\frac{1}{2}ik_x} e^{+\frac{\sqrt{3}}{2}ik_z^{(h)}} \right) \tag{94}$$

$$\varphi_{z;3}^{(h)} = \frac{1}{3}s^2 D^{(h)} + \frac{1}{6}K_\zeta \left(\frac{3}{2}D^{(h)} + \frac{\sqrt{3}}{4}\delta^p - \left(\frac{\sqrt{3}}{4}\delta^n e^{-\frac{1}{2}ik_x} + f_z^n \right) e^{+\frac{\sqrt{3}}{2}ik_z^{(h)}} \right) \tag{95}$$

For the right surface particle, these expressions are found as:

$$\varphi_{x;1}^{(h)} = \frac{1}{3}s^2 + \frac{1}{6}K_\zeta \left(\frac{3}{2} - e^{-ik_x} + \frac{1}{4}\delta^p - \left(\frac{1}{4}\delta^n e^{-\frac{1}{2}ik_x} + f_x^n \right) e^{+\frac{\sqrt{3}}{2}ik_z^{(h)}} \right) \tag{96}$$

$$\varphi_{x;2}^{(h)} = \frac{1}{3}s^2 + \frac{1}{6}K_\zeta \left(\frac{3}{2} - e^{-ik_x} + \frac{1}{4}\delta^n - \left(\frac{1}{4}\delta^p e^{-\frac{1}{2}ik_x} + f_x^n \right) e^{-\frac{\sqrt{3}}{2}ik_z^{(h)}} \right) \tag{97}$$

$$\varphi_{x;3}^{(h)} = \frac{1}{3}s^2 + \frac{1}{6}K_\zeta \left(\frac{3}{2} - e^{-ik_x} + \frac{1}{4}\delta^p - \left(\frac{1}{4}\delta^n e^{-\frac{1}{2}ik_x} + f_x^n \right) e^{+\frac{\sqrt{3}}{2}ik_z^{(h)}} \right) \tag{98}$$

$$\varphi_{z;1}^{(h)} = \frac{1}{3}s^2 D^{(h)} + \frac{1}{6}K_\zeta \left(\frac{3}{2}D^{(h)} + \frac{\sqrt{3}}{4}\delta^p - \left(\frac{\sqrt{3}}{4}\delta^n e^{-\frac{1}{2}ik_x} + f_z^n \right) e^{+\frac{\sqrt{3}}{2}ik_z^{(h)}} \right) \tag{99}$$

$$\varphi_{z;2}^{(h)} = -\frac{1}{3}s^2 D^{(h)} - \frac{1}{6}K_\zeta \left(\frac{3}{2}D^{(h)} - \frac{\sqrt{3}}{4}\delta^n + \left(\frac{\sqrt{3}}{4}\delta^n e^{-\frac{1}{2}ik_x} - f_z^n \right) e^{-\frac{\sqrt{3}}{2}ik_z^{(h)}} \right) \tag{100}$$

$$\varphi_{z;3}^{(h)} = \frac{1}{3}s^2 D^{(h)} + \frac{1}{6}K_\zeta \left(\frac{3}{2}D^{(h)} + \frac{\sqrt{3}}{4}\delta^p - \left(\frac{\sqrt{3}}{4}\delta^p e^{-\frac{1}{2}ik_x} + f_z^n \right) e^{+\frac{\sqrt{3}}{2}ik_z^{(h)}} \right) \tag{101}$$

Data availability

Data will be made available on request.

References

- [1] Wolf JP. *Dynamic soil-structure interaction*. Prentice-hall international series in civil engineering and engineering mechanics, Englewood Cliffs, New Jersey, United States of America: Prentice-Hall; 1985
- [2] Croasdale KR, Cammaert AB. An improved method for the calculation of ice loads on sloping structures in first-year ice. *Hydrotech Constr* 1994;28(3):174–9. <http://dx.doi.org/10.1007/BF01545935>.
- [3] Altan BS, Aifantis EC. On some aspects in the special theory of gradient elasticity. *J Mech Behav Mater* 1997;8(3):231–82. <http://dx.doi.org/10.1515/JMBM.1997.8.3.231>.
- [4] Askes H, Suiker ASJ, Sluys LJ. A classification of higher-order strain-gradient models – linear analysis. *Arch Appl Mech* 2002;72(2):171–88. <http://dx.doi.org/10.1007/s00419-002-0202-4>.
- [5] Chang CS, Gao J. Second-gradient constitutive theory for granular material with random packing structure. *Int J Solids Struct* 1995;32(16):2279–93. [http://dx.doi.org/10.1016/0020-7683\(94\)00259-Y](http://dx.doi.org/10.1016/0020-7683(94)00259-Y).
- [6] de Borst R, Mühlhaus HB. Gradient-dependent plasticity: Formulation and algorithmic aspects. *Internat J Numer Methods Engrg* 1992;35(3):521–39. <http://dx.doi.org/10.1002/nme.1620350307>.
- [7] Fleck NA, Hutchinson JW. A reformulation of strain gradient plasticity. *J Mech Phys Solids* 2001;49(10):2245–71. [http://dx.doi.org/10.1016/S0022-5096\(01\)00049-7](http://dx.doi.org/10.1016/S0022-5096(01)00049-7).
- [8] Metrikine AV, Askes H. An isotropic dynamically consistent gradient elasticity model derived from a 2D lattice. *Phil Mag* 2006;86(21–22):3259–86. <http://dx.doi.org/10.1080/14786430500197827>.
- [9] Slepyan LI. *Models and phenomena in fracture mechanics*. Foundations of engineering mechanics, Heidelberg: Springer Berlin; 2002. <http://dx.doi.org/10.1007/978-3-540-48010-5>.
- [10] Bolander JE, Eliáš J, Cusatis G, Nagai K. Discrete mechanical models of concrete fracture. *Eng Fract Mech* 2021;257:108030. <http://dx.doi.org/10.1016/j.engfracmech.2021.108030>.
- [11] Katsura S, Morita T, Inawashiro S, Horiguchi T, Abe Y. Lattice Green’s function. Introduction. *J Math Phys* 1971;12(5):892–5. <http://dx.doi.org/10.1063/1.1665662>.
- [12] Maradudin AA, Montroll EM, Weiss GH, Ipatova IP. *Theory of lattice dynamics in the harmonic approximation*. Solid state physics. 2nd ed. New York and London: Academic Press; 1971.
- [13] Martin PA. Discrete scattering theory: Green’s function for a square lattice. *Wave Motion* 2006;43(7):619–29. <http://dx.doi.org/10.1016/j.wavemoti.2006.05.006>.
- [14] Cai W, de Koning M, Bulatov VV, Yip S. Minimizing boundary reflections in coupled-domain simulations. *Phys Rev Lett* 2000;85(15):3213–6. <http://dx.doi.org/10.1103/PhysRevLett.85.3213>.
- [15] Karpov EG, Wagner GJ, Liu WK. A Greens function approach to deriving non-reflecting boundary conditions. *Internat J Numer Methods Engrg* 2005;62:1250–62. <http://dx.doi.org/10.1002/nme.1234>.
- [16] Carpio A, Tapiador B. Nonreflecting boundary conditions for discrete waves. *J Comput Phys* 2010;229(5):1879–96. <http://dx.doi.org/10.1016/j.jcp.2009.11.013>.
- [17] de Oliveira Barbosa JM, Färågåu AB, van Dalen KN. A lattice model for transition zones in ballasted railway tracks. *J Sound Vib* 2021;494:115840. <http://dx.doi.org/10.1016/j.jsv.2020.115840>.
- [18] Kausel E, Barbosa JM de Oliveira. PMLs: A direct approach. *Internat J Numer Methods Engrg* 2012;90(3):343–52. <http://dx.doi.org/10.1002/nme.3322>.
- [19] Friedman MB, Shaw RP. Diffraction of pulses by cylindrical obstacles of arbitrary cross-section. *J Appl Mech* 1962;29:40–6. <http://dx.doi.org/10.1115/1.3636495>.
- [20] Banaugh RP, Goldsmith W. Diffraction of steady elastic waves by surfaces of arbitrary shape. *J Appl Mech* 1963;30:589–97. <http://dx.doi.org/10.1115/1.3636624>.
- [21] Dominguez J. *Boundary elements in dynamics*. London: Computational mechanics publications; 1993.
- [22] de Hoop AT. An elastodynamic reciprocity theorem for linear, viscoelastic media. *Appl Sci Res* 1966;16(1):39–45. <http://dx.doi.org/10.1007/BF00384053>.

- [23] Huygens C. *Traité de la Lumière*. Leiden: Pierre vander Aa; 1690, <http://dx.doi.org/10.5479/sil.294285.39088000545160>.
- [24] Lanczos C. *The variational principles of mechanics*. 3rd ed. Toronto: University of Toronto Press; 1966.
- [25] Landau LD, Lifshitz EM. *Mechanics*. Oxford: Pargamon; 1976.
- [26] Suiker ASJ, Metrikine AV, de Borst R. Comparison of wave propagation characteristics of the cosserat continuum model and corresponding discrete lattice models. *Int J Solids Struct* 2001;38:1563–83. [http://dx.doi.org/10.1016/S0020-7683\(00\)00104-9](http://dx.doi.org/10.1016/S0020-7683(00)00104-9).
- [27] Askes H, Metrikine AV. Higher-order continua derived from discrete media: continualisation aspects and boundary conditions. *Int J Solids Struct* 2004;42:187–202. <http://dx.doi.org/10.1016/j.ijsolstr.2004.04.005>.
- [28] Suiker ASJ, Metrikine AV, de Borst R. Dynamic behaviour of a layer of discrete particles, part 1: Analysis of body waves and eigenmodes. *J Sound Vib* 2001;240:1–18. <http://dx.doi.org/10.1006/jsvi.2000.3202>.
- [29] Brillouin L. *Wave propagation in periodic structures: electric filters and crystal lattices*. 2nd ed. New York, NY: Dover; 1953.
- [30] Abramowitz M, Stegun IA. *Handbook of mathematical functions with formulas, graphs, and mathematical tables*, 9th printing. New York: Dover; 1972.
- [31] Woods FS. Differentiation of a definite integral. In: *Advanced calculus: a course arranged with special reference to the needs of students of applied mathematics*. Boston, MA: Ginn; 1926, p. 141–4.
- [32] Pan Z, Ma R, Wang D, Chen A. A review of lattice type model in fracture mechanics: theory, applications, and perspectives. *Eng Fract Mech* 2018;190:382–409. <http://dx.doi.org/10.1016/j.engfracmech.2017.12.037>.